NUMERICAL SIMULATION OF UNSTEADY NORMAL DETONATION COMBUSTION

by

AJJAY OMPRAKAS

Presented to the Faculty of the Graduate School of

The University of Texas at Arlington in Partial Fulfillment

of the Requirements

for the Degree of

MASTER OF SCIENCE IN AEROSPACE ENGINEERING

THE UNIVERSITY OF TEXAS AT ARLINGTON

MAY 2018

Acknowledgments

This thesis would not have been possible without the guidance and help of all my supervisor, professors, lab mates, family and friends. I would like to thank my masters supervisor Dr Donald R Wilson and PhD mentor Rahul Kumar who guided me throughout the project, without whom this thesis would not have been possible. I would like to thank Dr. Endel v larve and Dr Miguel A Amaya for agreeing to be on the defense committee and reviewing my thesis.

Finally, I would like to thank my family and friends for their continued support and encouragement throughout my education and stay in UTA.

May 09, 2018

ABSTRACT

NUMERICAL SIMULATION OF UNSTEADY NORMAL DETONATION COMBUSTION

AJJAY OMPRAKAS, M.S

The University of Texas at Arlington, 2018

Supervising Professor: Donald R Wilson

The objective of this research is to simulate normal detonation combustion which is a mode of operation for a Pulsed Detonation Engine (PDE). A supersonic flow with stoichiometric hydrogen-air mixture is made to impinge on a wedge, thus resulting in increasing the temperature and pressure across a shock wave leading to the formation of detonation wave. Different modes of the operations can be simulated by varying the incoming Mach number, pressure, temperature and equivalence ratio. For the case of normal detonation wave mode which is an unsteady process, after the detonation being initiated due to the shock induced by the wedge, the detonation wave propagates upstream in the flow as the combustion chamber Mach number is lower than the C-J Mach number. The concept of detonation wave moving upstream and downstream is controlled by changing the incoming flow field properties. By this method the unsteady normal detonation wave is made to oscillate in the combustion chamber leading to a continuous detonation combustion. The intention of this research is to simulate two cycles of detonation combustion in order to determine the frequency and to obtain the variation of flow properties at the exit plain with respect to time.

TABLE OF CONTENTS

List of Illustrations

List of Tables

Chapter 1

INTRODUCTION

1.1 Concept of Multi-Mode Pulsed Detonation Engine

The Pulse Detonation Engine (PDE) has created considerable attention due to its higher thrust potential, wider operating range, high thermodynamic efficiency and its mechanical simplicity with the lack of movable parts compared to the conventional engine[1][2]. The advantages of the PDE comes from its utilization of the detonation combustion rather than regular deflagration that has been used by the Brayton cycle engines. The detonation process is much more energetic than deflagration combustion, consisting of a shock wave propagating at supersonic speed coupled with an induction and reaction zone, whereas in a deflagration the combustion occurs at subsonic speed.[1][2][3].

But the conventional PDE cannot be operated at hypersonic speed since the inlet compression increases the static temperature to a value greater than the autoignition temperature of the fuel. To overcome this difficulty the concept of the multi-mode pulsed detonation engine was conceptualized by considering the best features of various engine concepts such that it can overcome the limitations of the individual engine concepts and provide the ability to operate over a wide range of operating conditions from subsonic to supersonic speed. This concept is illustrated

in the Fig 1.1, and it consists of four modes of operations. The operating modes are as follows - (a) an ejector-augmented pulsed detonation rocket (PDR) mode for take-off and accelerate to moderate supersonic velocity, (b) a normal detonation wave engine (NDWE) mode for operation at flight Mach numbers from approximately 3 to 6 where the combustion chamber Mach number is less than the a Chapman-Jouguet Mach number for the given fuel stoichiometry condition, (c) an oblique detonation wave engine (ODWE) mode for hypersonic flight where the combustion chamber Mach number is greater than that of the Chapman-Jouguet Mach number for a given fuel stoichiometry condition and (d) a pulsed detonation rocket mode for very high Mach number and altitude due to the scarcity of oxygen for combustion[4][1][5][6].

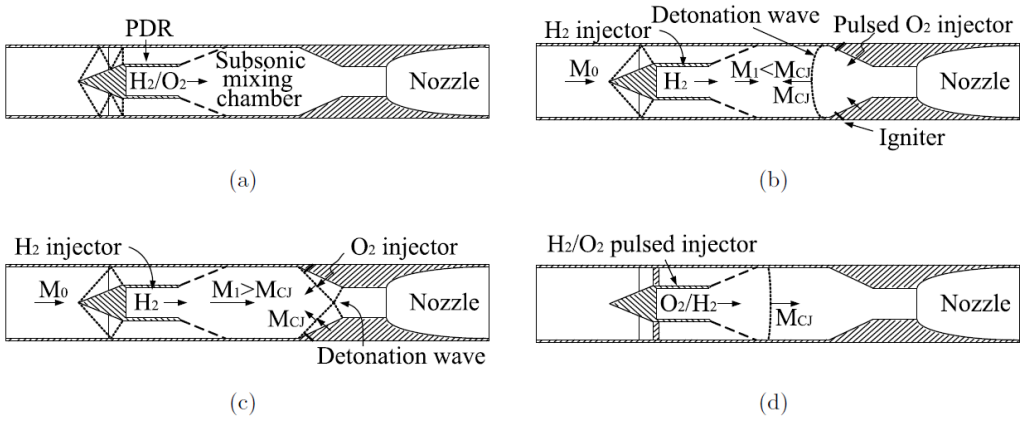

Fig 1.1 : Multimode pulse detonation engine

1.2 Detonation Physics and Chapman – Jouguet condition

A detonation wave is a complex oscillating three-dimensional cellular structure consisting of a shock followed by an induction zone with a coupled reaction region where the products are accompanied by a rapid release of energy. As the detonation wave propagation is supersonic in nature, the reactants upstream are not affected until the flow comes in contact with the detonation wave front. As the shock passes through the reactants it compresses, heats and ignites the mixture resulting in combustion zone propagating with the velocity of the shock. The shock wave is coupled with the reaction zone, triple point, transverse wave and shear layer as shown in the Fig 1.2 (a,b) [4][6][1][2][3]. Consider a detonation wave propagating in a tube filled with a combustible mixture that is closed at one end and opened at the other. The detonation is initiated at the closed end by a high enthalpy source, and the shock wave moves at the velocity of the detonation wave V_{det} relative to the gas chamber. The thermodynamics of the process is given by T-S diagram as shown in Fig 1.3

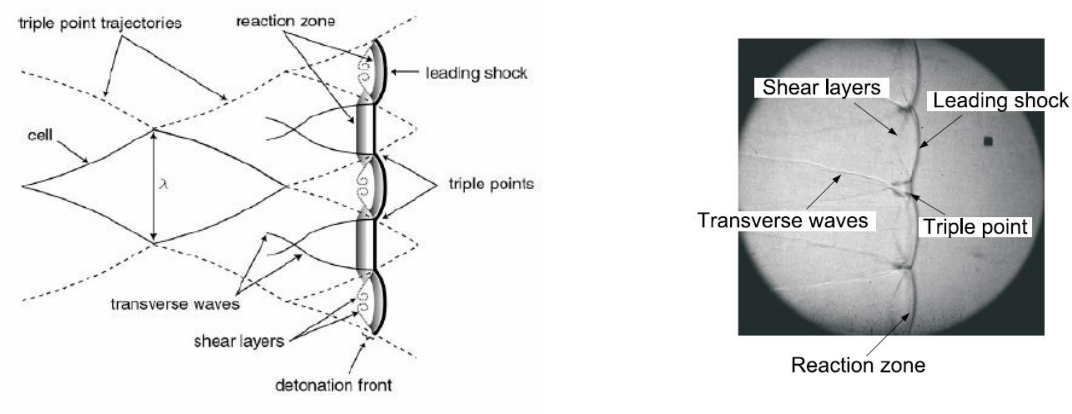

Fig 1.2 (a,b) : schematics of detonation

Fig 1.3 shows the difference between the constant pressure combustion (Brayton cycle), constant volume combustion (Humphrey cycle) and detonation cycle. The stage 0 -1 known as the pre-compression is mandatory for a Brayton cycle but for detonation the leading shock provides the necessary pressure rise to sustain the combustion.

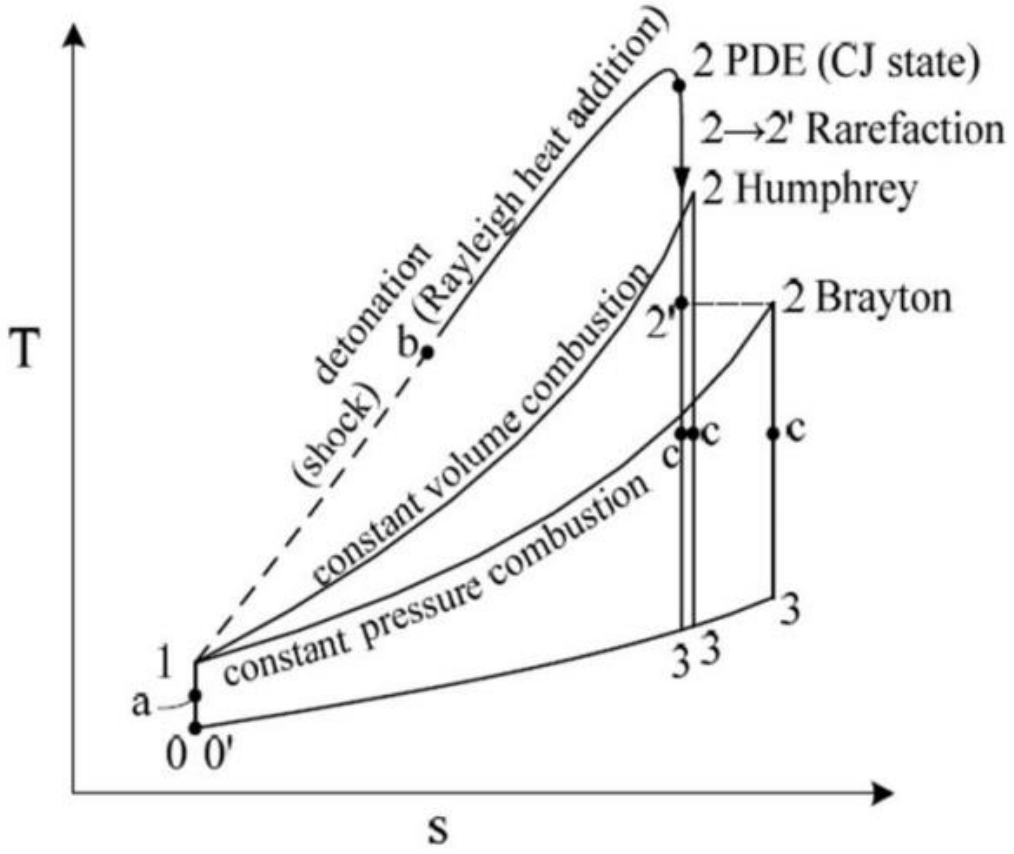

Fig 1. 3 : T-S diagram for different combustion model

This complex concept of detonation is explained by two relatively simple theoretical model: The Chapman-Jouguet (CJ) and Zeldovich-von Neumann-Döring (ZND) models. The first theory of detonation was proposed by Chapman in 1899 and followed by Jouguet in 1905. In this theory it is assumed that the chemical reaction takes place instantaneously inside the shock and the reaction zone length shrink to zero as shown in Fig 1.4. The products are assumed to flow at a local sonic velocity relative to the shock, which is called as the Chapman – Jouguet condition.

In this case the velocity of the products can be obtained by the one-dimensional conservation equation of mass, momentum and energy coupled with the chemical reaction

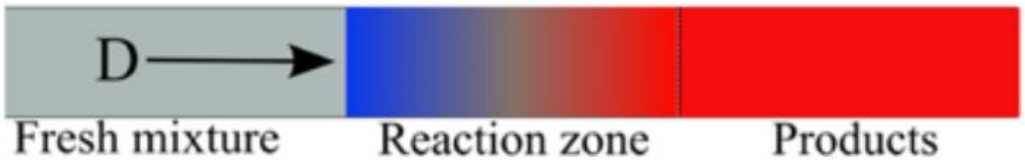

Fig 1.4: Chapman – Jouguet Detonation model

An improved and more modern theory that takes into the account the effect of the finite rate chemical reactions was originated from the work of Zel'dovich, von Neumann, and Doering in 1940's, which was later named as the ZND theory. This model of detonation is assumed to have a strong shock wave that is been coupled to a reaction zone where a fuel and oxidizer mixture is compressed by the leading shock and is rapidly burned, which releases energy that is utilized to sustain the propagating shock. The leading shock travels at the detonation velocity, and the strength of the shock depends on the detonation velocity. In this the reaction zone is divided into two regions, namely an induction zone and the heat addition zone. In the induction zone the reaction is delayed due to the finite time required to initiate the chemical reaction. The energy is released in the heat addition zone after the

reaction begins. From Fig 1.5, A pressure spike is observed in the induction zone and it is referred as the Von Neumann pressure spike [2][4][3].

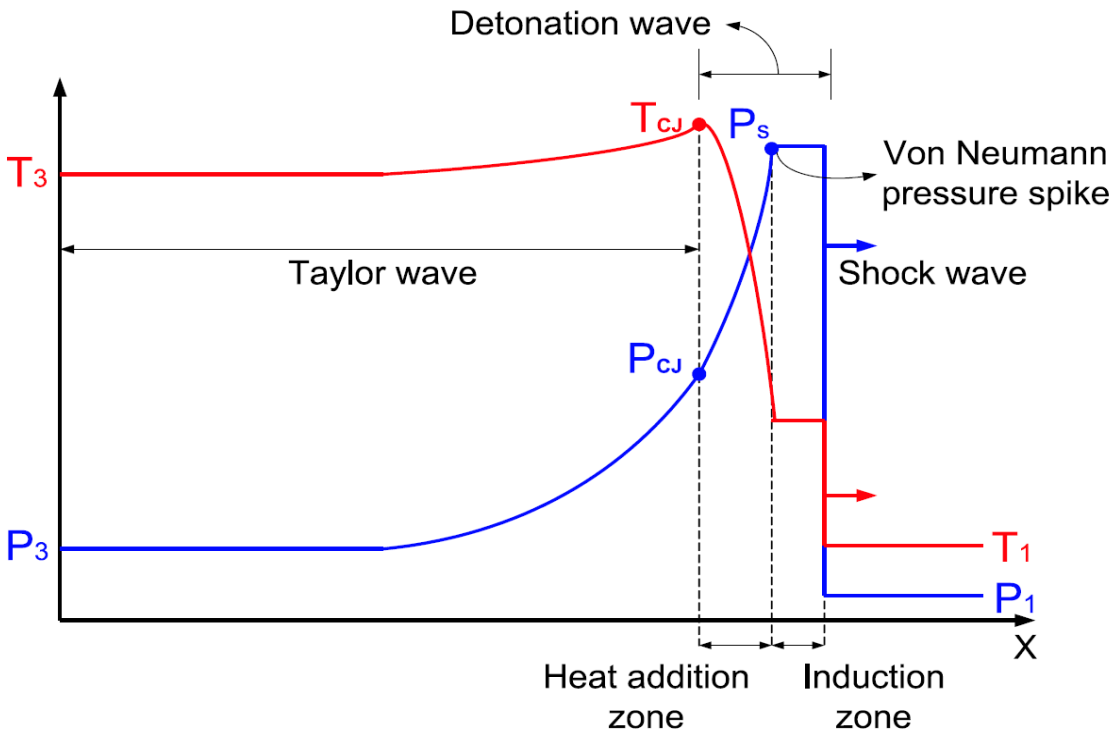

Fig 1.5: Variation of Pressure and temperature in ZND Detonation.

The concept of highly energetic detonation phenomena can be applied to the propulsion system. One such concept of engine is the pulsed detonation engine (PDE), that was first introduced during the late 1940's. The ideal advantage of PDE over the engine that follows a Brayton cycle is the high thermodynamic efficiency that's possible to achieve by controlled combustion through detonation cycle. Fig 1.6 represents the concept of a PDE with a nozzle at the end to expand the combusted gas. A generic PDE cycle consist of four different steps, (a) filling of

fuel-oxidizer mixture, (b) initiating the detonation, (c) detonation propagation and (d) purging of the burned gas in a blowdown process.

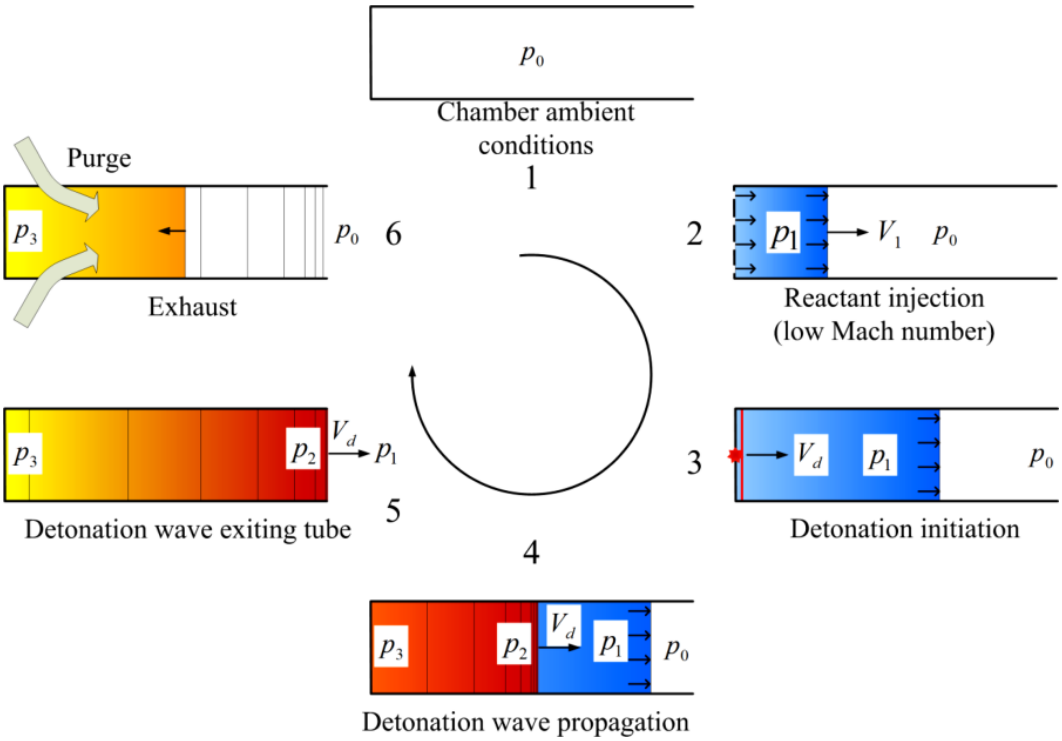

Fig 1.6: Pulsed detonation engine cycle

The PDE cycle begins with the detonation chamber being filled with the fuel-oxidizer mixture through the valve opening. In the Fig 1.6 p_0 and p_1 are the ambient and mixture pressure respectively. As the detonation velocity is higher than the velocity of fuel-oxidizer velocity during the filling process, the detonation is initiated before the mixture reaches the end of the chamber using an ignitor. An unsteady expansion wave is generated behind the detonation wave as it propagates through the combustion medium, which explains the pressure of the burned gas being less than the Von Neumann pressure[6][7][16]. An ideal detonation wave

will propagate at the Chapman Jouguet (CJ) velocity for the given mixture initial condition. As soon as the detonation exits the chamber a blowdown process is started due to the pressure difference across the exit plane of the chamber, which is then followed by a purging process that's basically injecting relatively cool air into the chamber to clear out the burned gas and to cool the chamber in order to prevent auto-ignition of the fresh fuel-oxidizer mixture that gets injected in the following cycle.

1.3 Thermodynamics

In order to understand the detonation, process, a detailed analysis of thermodynamics is needed. For the analysis a steady state control volume of a detonation is considered that is shown in the Fig 1.7. By applying the continuity, momentum and energy equation with a fluid behaving as an ideal gas to the control volume represented in the Fig 1.7, gives the following [17][4][14]

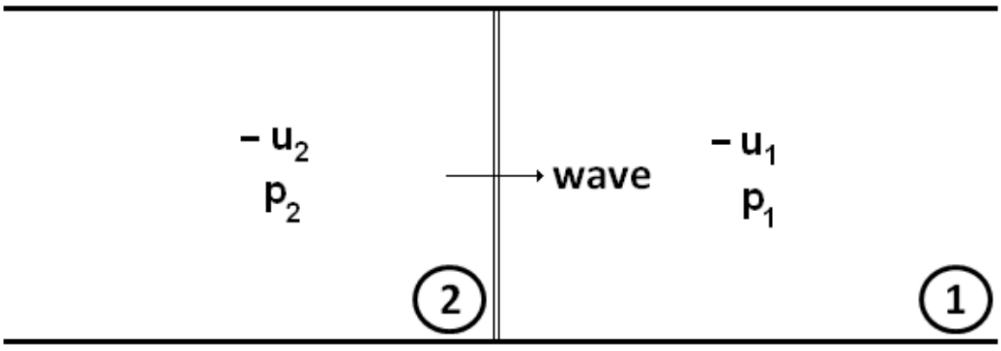

Fig 1.7 : Flow properties across a detonation

$$\rho_1 * u_1 = \rho_2 * u_2 \tag{1.1}$$

$$p_1 + \rho_1 u_1^2 = p_2 + \rho_2 u_2^2 \tag{1.2}$$

$$c_{p,1} T_1 + \frac{1}{2} u_1^2 + q = c_{p,2} T_2 + \frac{1}{2} u_2^2 \tag{1.3}$$

$$p_1 = \rho_1 R_1 T_1 \tag{1.4}$$

$$p_2 = \rho_2 R_2 T_2 \tag{1.5}$$

In these equations the heat addition because of the chemical reaction is accounted by the term q. The total enthalpy of the mixture is defined as $h = c_p T + h^o$. In the above equation the heat addition is accounted by the term $q = h_2 - h_1$.

The equation that relates the thermodynamics properties across the discontinuity is obtained by simplifying the Rankine – Hugoniot equation [**2**][3][17]

$$h_2 - h_1 = \frac{1}{2} \left(\frac{1}{\rho_2} - \frac{1}{\rho_1} \right) (p_2 - p_1) \tag{1.6}$$

which is simplified to

$$\frac{1}{\gamma - 1}\,(p_2 v_2 - p_1 v_1) - \frac{1}{2}\,(p_2 - p_1)(v_2 + v_1) - q = 0 \tag{1.7}$$

The Rankine – Hugoniot curve is represented in the Eq. 1.7. It is important to plot the Hugoniot equation in terms of (p, υ) as total enthalpy is a function of (p, ρ) and the solution lies in this plane regardless of the flow velocity. The Rankine – Hugoniot curve is given in the Fig 1.8 (a) and (b). The line that is tangential to the Rankine – Hugoniot curve is the Rayleigh line representing mass flux from the Eq. 1.8.

$$\frac{(p_2 - p_1)}{\left(\frac{1}{\rho_2} - \frac{1}{\rho_1}\right)} = -\dot{m}^{''} \tag{1.8}$$

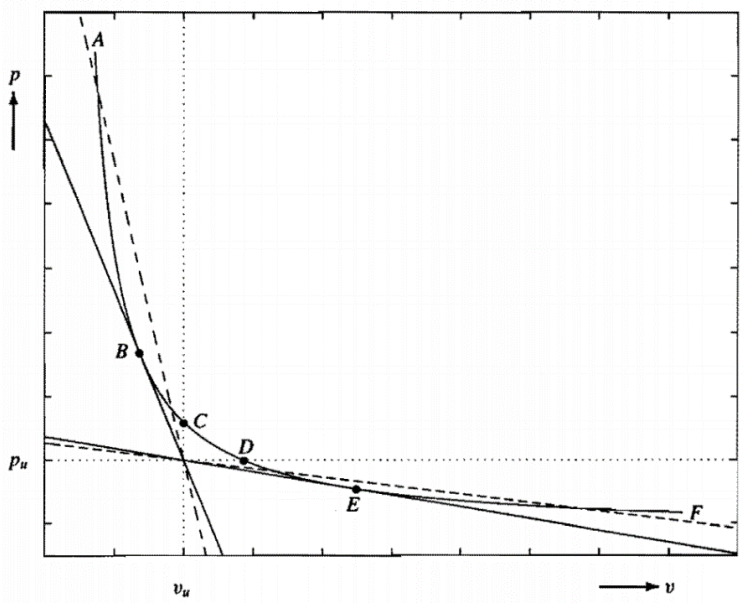

Fig 1.8: (a) Rankine – Hugoniot curve

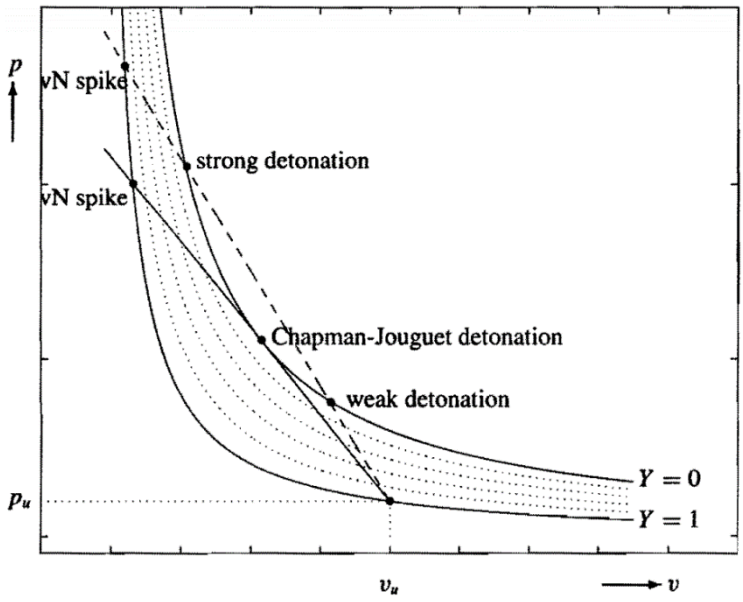

Fig 1.8: (B) Rankine – Hugoniot curve to calculate von Neumann pressure spike

The point on the Hugoniot curve where the Rayleigh line is tangential to each other is known as the Chapman – Jouguet (CJ) point. Theoretically there are two CJ points on a Hugoniot curve, the upper CJ point (CJ_u) and the lower CJ point (CJ_l). They are located respectively where the Raleigh line is tangential to the Hugoniot curve on the detonation and deflagration branch. The Hugoniot curve is divided into five regions and is represented in the Table 1.1.

Regions in Hugoniot	**Characteristics**	**Burned gas velocity**
Region 1 (A - B)	Strong Detonation	Subsonic
Region 2 (B - C)	Weak Detonation	Supersonic
Region 3 (C -D)	The relation is not satisfied	
Region 4 (D - E)	Weak deflagration	Subsonic
Region 5 (E and F)	Strong deflagration	supersonic

Table 1.1 – Regions in Hugoniot curve

Starting from region 3 any region upstream and downstream of the given region satisfies the Rayleigh and Hugoniot relations that is been represented in the Eq. 1.8 and Eq. 1.7 respectively. The region 3 does not represent any real solution for the equation. In this case between the region 2 and 4 no valid Rayleigh lines could be drawn.

The regions 1 and 2 corresponds to strong and weak detonation regions respectively, the region 4 and 5 represents the weak and strong deflagration respectively. In case of a detonation the gas dynamic properties of the fluid are needed to determine the burned gas propagating speed, that's independent of the actual structure of the wave. This discovery was initially made by Chapman and Jouguet in the early 20^{th} century. It was Chapman who postulated that solution points are when the Rayleigh line is tangential to the Hugoniot curve.

The region 1 represents the conditions required for a strong detonation. In this case the burned gas will be of subsonic Mach number referenced to the local temperature. The gas behind the detonation will still follow up the detonation at CJ velocity. The region 2 represents the conditions for a weak detonation with burned gas having a supersonic Mach number. The region 4 and 5 represents the condition to have a deflagration. In case of deflagration the propagating speed is determined by the transport properties of the gasses. The region 4 is a weak deflagration and the region 5 is a strong deflagration. [4][3]. The conditions at the point B is the upper C-J point and the point E represents the lower C-J point.

By calculating the entropy at the C-J points for a given stoichiometry. It can be observed that a higher entropy is achieved for the conditions corresponding to the

upper C-J point. And a lower entropy value is obtained from the conditions that corresponds to the lower C-J point.

The major importance of C-J theory is to obtain the detonation flow properties. The C-J wave propagation speed was experimentally measured by Winterberger in 2004 and found to be within a range of 2% with the theoretical CJ theory. The detonation temperature is given by [3][17]

$$T_d = \frac{\gamma_d}{2\gamma_d + 1}\left(\frac{C_{p,u}}{C_{p,d}}\,T_u + \frac{q}{C_{p,d}}\right) \tag{1.9}$$

The detonation velocity for a real gas, V_d is represented as

$$V_d = \sqrt{2(\gamma_d + 1)\gamma_d\, R_d\left(\frac{C_{p,a}}{C_{p,d}}\,T_u + \frac{q}{C_{p,d}}\right)} \tag{1.10}$$

When the downstream fluid is of CJ condition then the Eq. (1.10) can be written as

$$V_{CJ} = \frac{\rho_{CJ}}{\rho_u}\sqrt{\gamma_{CJ}\, R_{CJ}\, T_{CJ}} \tag{1.11}$$

Chapter 2

GOVERNING EQUATIONS

To simulate of a flow with a reacting gas mixture, the chemical reaction between the gases need to be modeled together with the fluid dynamics. For example, in the case of detonation or combustion, the basic equations of the reactive flow are the conservation of the mass, energy and momentum along with the change in composition of gas mixture due to reaction.[4][5][17]

2.1 Reactive Euler equation

Ignoring viscosity, heat transfer, diffusion, radiation and body forces, the governing equation for a compressible reactive flow are the reactive Euler equation [4][17][25]. The axisymmetric reactive Euler equation are used for modeling the PDEs combustion chamber. In actuality the detonation is characterized by a three-dimensional cellular structure, which these equations lack the physical makeup to capture. Since the research is to identify the gas dynamic of various flow features, the axisymmetric model representation will work for our case. The reactive Euler equation are given by

$$\frac{\partial \boldsymbol{Q}}{\partial t} + \frac{\partial \boldsymbol{F}}{\partial x} + \frac{\partial \boldsymbol{G}}{\partial r} + \boldsymbol{H} = \boldsymbol{W} \tag{2.1}$$

where the state vector **Q,** flux vector in the x-direction **F**, flux vector in r-direction **G**, axisymmetric term **H**, and the species source term **W**, are defined as

$$\boldsymbol{Q} = \begin{bmatrix} \rho \\ \rho V_x \\ \rho V_r \\ \rho E \\ \rho Y_i \end{bmatrix},$$

$$\boldsymbol{F} = \begin{bmatrix} \rho_i V_x \\ \rho V_x^2 + p \\ \rho V_x V_r \\ (\rho E + p) V_x \\ \rho V_x Y_i \end{bmatrix},$$

$$\boldsymbol{G} = \begin{bmatrix} \rho_i V_x \\ \rho V_x V_r \\ \rho V_r^2 \\ (\rho E + p) V_r \\ \rho V_r Y_i \end{bmatrix}, \tag{2.2}$$

$$\boldsymbol{H} = \frac{1}{r} \begin{bmatrix} \rho_i V_r \\ \rho V_x V_r \\ \rho V_r^2 \\ (\rho E + p) V_r \\ \rho V_r Y_i \end{bmatrix},$$

$$\boldsymbol{W} = \begin{bmatrix} 0 \\ 0 \\ 0 \\ 0 \\ R_i \end{bmatrix},$$

Here ρ, V, E and p are the density, velocity, total energy per unit mass and the pressure of the fluid respectively. R_i corresponds to the net rate of production of an individual species due to chemical reaction. and i = 1…., N_s where N_s is the number of species. The Eq. 2.2 inherits gas dynamics and chemical reaction coupling that is required for modeling a self-sustained detonation.

The assumptions made in the 2-D reactive Euler equations are the external forces like gravity are negligible as the force is small in a hypersonic combustion but not in a low-speed combustion. The mass diffusion due to thermal and pressure difference and the heat transfer due to radiation and concentration difference known as the Dufour effect is assumed to be negligible.

The 1^{st} term represents the continuity term for the flow and gas dynamics property. The last row of the source terms in Eq. (2.2) represents the species continuity in the mixture that is valid for a finite reaction rate. The $2^{nd,}$ 3^{rd} and 4^{th} row corresponds to the momentum in the x-direction and r-direction and the energy equation respectively. And the pressure and temperature diffusivity terms are neglected since they are usually exceedingly small. The Eq. (2.2) describes large class of combustion problems, that are generally quite complex.

We introduce a preconditioned pseudo-time-derivative term in Eq. (2.1) as,

$$\frac{\delta}{\delta\tau}\int_V \boldsymbol{Q}\, dV + \oint [\boldsymbol{F}+\boldsymbol{G}]\,.\,dA + \int_V \boldsymbol{H}\, dV = \frac{\delta}{\delta t}\int_V \boldsymbol{W}\, dV \tag{2.3}$$

where t denotes the physical time step and τ denotes the pseudo-time used in the time-marching procedure. When τ tents to infinity Eq. (1.3) will be the same as Eq. (1.1). The time-dependent term in Eq. (1.3) is discretized in an implicit fashion by a Second-order accurate, backward difference in time. The dual time formulation is written in semi-discrete form as follows

$$\left[\frac{\Gamma}{\Delta\tau} + \frac{\epsilon_0}{\Delta t}\frac{\delta \boldsymbol{W}}{\delta \boldsymbol{Q}}\right] + \oint [\boldsymbol{F}+\boldsymbol{G}]\,.\,dA + \int_V \boldsymbol{H}\, dV = \frac{1}{\Delta t}(\epsilon_0 \boldsymbol{W}^k - \epsilon_1 \boldsymbol{W}^n + \epsilon_2 \boldsymbol{W}^{n-1}) \tag{2.4}$$

2.2 Thermodynamics Relation

Species and Mixture: The gas mixture as a whole is an ideal gas and the properties are functions of both temperature and pressure due to rapid change in chemical composition. In terms of individual species, they are considered to be thermally perfect gas. [6][10][13]

$$c_p \; is \; a \; function \; of \; Temperature \tag{2.5}$$

$$c_v \; is \; a \; function \; of \; Temperature \tag{2.6}$$

The enthalpy and internal energy of species are given by

$$h_i = h_i^f + \int_{T_0}^{T} c_{pi} \, dt \tag{2.7}$$

$$e_i = h_i^f + \int_{T_0}^{T} c_{vi} \, dt \tag{2.8}$$

where h_i^f is the heat of formation of the ith species at a reference temperature 298.15K also known as the heat of formation and is normally obtained from the thermodynamics database.

The above equations Eq. (2.7), and Eq. (2.8) are standard form for an arbitrary – order polynomial. The general form of the molar specific heat works with the thermodynamic data in the form used in the NASA CEA. In this case, seven coefficients are needed for polynomial function of temperature. This is expressed in the following form

$$\frac{C_{pi}}{R} = a_1 T^{-2} + a_2 T^{-1} + a_3 + a_4 T^1 + a_5 T^2 + a_6 T^3 + a_7 T^4 \tag{2.9}$$

The molar enthalpy is given as

$$\frac{H_i}{RT} = -a_1 T^{-2} + a_2 T^{-1} lnT + a_3 + a_4 \frac{T}{2} + a_5 \frac{T^2}{3} + a_6 \frac{T^3}{4} + a_7 \frac{T^4}{5} + \frac{a_8}{T} \quad (2.10)$$

The entropy of the species is calculated by

$$\frac{S_i}{R} = -a_1 \frac{T^{-2}}{2} - a_2 T^{-1} + a_3 lnT + a_4 T + a_5 \frac{T^2}{2} + a_6 \frac{T^3}{3} + a_7 \frac{T^4}{4} + a_9 \quad (2.11)$$

The coefficients a_1 to a_9 in Eq. 2.9 – 2.11 are obtained from the thermodynamics database that takes into account the rotational and vibrational energy of the species over a temperature range from 200 K to 6000 K. From the above equation Eq. (2.8)-(2.11), the specific heat and enthalpy of the species per unit mass are a function of temperature, and are given by

$$c_{pi} = \frac{R}{W_i} C_{pi} \quad (2.12)$$

$$h_i = \frac{RT}{W_i} H_i \quad (2.13)$$

The specific heat at constant volume and internal energy is given by

$$c_{vi} = c_{pi} - \frac{R}{W_i} \tag{2.14}$$

$$e_i = h_i - \frac{RT}{W_i} \tag{2.15}$$

By taking the summation of i from 1 to N_s, the above four equations will provide the thermodynamic properties of the fluid such as the specific heat at constant pressure, enthalpy, specific heat at constant volume and entropy.

Ideal gas equation: The equation of state for an ideal gas is given by,

$$P = \sum_{i=1}^{N_s} \rho R_i T \tag{2.16}$$

where

$$R_i = \frac{R}{W_i} \tag{2.17}$$

where R is the universal gas constant (8314 J/ mol · K) and ρ is the total density of the mixture.

The speed of sound is given by

$$\boldsymbol{C} = \sqrt{\gamma RT} = \sqrt{\frac{\gamma P}{\rho}} \tag{2.18}$$

Where γ is the ratio of specific heat.

2.3 Chemical Kinetics

A detailed and a stable chemical model is necessary for the source term in Eq. 2.2 is necessary in order to create an accurate numerical model of detonation. Due to rapid chemical reaction in the case a detonation right behind the shock discontinuity creates stiffness in source terms. To overcome the stiffness in the source term due to chemical reaction and the chemical non-equilibrium the entire source terms need to be solved simultaneously.

Chemical Reaction Mechanism: Taking the stoichiometry reaction of hydrogen-air, the balanced chemical reaction equation is given as,

$$2H_2 + (O_2 + 3.762\ N_2) \rightarrow 2H_2O + 3.762\ N_2 \qquad (2.19)$$

To attain this reaction, a series of elementary reaction which represented in a step by step sequence by which the overall reaction takes place is named as the chemical reaction mechanism. The reaction mechanism consists of the information regarding reaction rate, third body and pressure depended reaction that represents the accurate reaction mechanism as a whole. Combining all the elementary reactions will give

rise to the detailed reaction with lower chemical stiffness that will be used for the numerical simulation of detonation wave.

The hydrogen-air mechanism is represented in various detailed levels from a single step, two steps to a detailed 268 step reaction mechanism [11]. In this study, a 11 species and 23 step hydrogen-air model that's shown in Table.1 is employed as a good representation of the hydrogen-air mechanism for the required operating condition.

The general form of the chemical reaction is written in a compact form as,

$$\sum_{i=1}^{N_s} v'_{ij} M_i \leftrightarrow \sum_{i=1}^{N_s} v''_{ij} M_i \tag{2.20}$$

where i and j are the number of species and number of reactions respectively. In this relation, v'_{ij} and v''_{ij} represents the stoichiometric coefficient of the reactants and products respectively.

From the elementary reactions, the net rate of production of a given species is given by,

$$\dot{R}_i = \sum_{j=1}^{N_r} \left(v''_{ij} - v'_{ij}\right) \left\{ k_{f,j} \prod_{i=1}^{N_s} [M_i]^{v''_{ij}} - k_{b,j} \prod_{i=1}^{N_s} [M_i]^{v'_{ij}} \right\} \tag{2.21}$$

In this relation, the forward reaction rate is given by $k_{f,j}$ for the j[th] reaction which is obtained through the Arrhenius equation [11][10][17]

$$k_{f,j} = A_r T^n e^{-\frac{E_r}{RT}} \tag{2.22}$$

and the backward reaction rate is given by

$$k_{b,j} = \frac{k_{f,j}}{k_{c,j}} \tag{2.23}$$

where

$$k_{c,j} = k_{p,j} \left(\frac{P_{atm}}{RT}\right)^{\Sigma_{i=1}^{N_s}\left(\upsilon_{ij}^{"} - \upsilon_{ij}^{'}\right)} \tag{2.24}$$

$$k_{p,j} = exp\left[\sum_{i=1}^{N_s}\left(\upsilon_{ij}^{"} - \upsilon_{ij}^{'}\right)\left(\frac{S_i}{R} - \frac{H_i}{RT}\right)\right] \tag{2.25}$$

The term A_r is the pre-exponential factor, n is the temperature exponent and E_r is the activation energy. The values are given in Table 2.1 for hydrogen-air reaction. The backward reaction rate $k_{b,j}$ in Eq. 2.23 is determined by the forward reaction rate and the equilibrium constant. The equilibrium constant $k_{c,j}$ is determined from the Eq. 2.24 and Eq. 2.25. P_{atm} represents the sea level atmospheric pressure and the terms $\frac{H_i}{RT}$ and $\frac{S_i}{R}$ are derived from the Eq. 2.10 and Eq. 2.11 respectively.

REACTION MECHANISM	A mole-cm-sec-K	b	E cal/mole
H2 + O2 <=> OH + OH	1.70E+13	0	47780
OH + H2 <=> H2O + H	1.17E+09	1.3	3626
O + OH <=> O2 + H	4.00E+14	-0.5	0
O + H2 <=> OH + H	5.06E+04	2.67	6290
H + O2 + M <=> HO2 + M H2O enhanced by 18.6 H2 enhanced by 2.86 N2 enhanced by 1.26	3.61E+17	-0.72	0
OH + HO2 <=> H2O + O2	7.50E+12	0	0
H + HO2 <=> OH + OH	1.40E+14	0	1073
O + HO2 <=> O2 + OH	1.40E+13	0	1073
OH + OH <=> O + H2O	6.09E+08	1.3	0
H + H + M <=> H2 + M H2O enhanced by 0.0 H2 enhanced by 0.0	1.00E+18	-1.0	0
H + H + H2 <=> H2 + H2	9.20E+16	-0.6	0
H + H + H2O <=> H2 + H2O	6.00E+19	-1.25	0
H + OH + M <=> H2O + M H2O enhanced by 5.0	1.60E+22	-2	0
H + O + M <=> OH + M H2O enhanced by 5.0	6.20E+16	-0.6	0
O + O + M <=> O2 + M	1.89E+13	0	-1788
H + HO2 <=> H2 + O2	1.25E+13	0	0
HO2 + HO2 <=> H2O2 + O2	2.00E+12	0	0
H2O2 + M <=> OH + OH + M	1.30E+17	0	45500
H2O2 + H <=> HO2 + H2	1.60E+12	0	3800
H2O2 + OH <=> H2O + HO2	1.00E+13	0	1800
O + N2 <=> NO + N	1.40E+14	0	75800
N + O2 <=> NO + O	6.40E+09	1	6280
OH + N <=> NO + H	4.00E+13	0	0

Table 2.1: Reaction mechanism of Hydrogen -air

Third Body Reactions: These reactions tend to appear in the detailed reaction mechanism when the reactants or products is having higher bonding energy. An example for a third body reaction is

$$H + O_2 + M \leftrightarrow HO_2 + M \tag{2.26}$$

where M the third body could be H_2O, H_2, N_2 . In this the energy released from the formation of HO_2 from H and O_2 is carried out with the help of the third body. In the backward reaction the third body provides the required amount of energy to break the bond in HO_2 to give rise to H and O_2.[4][10][6]. The molar concentration with the third body efficiency is given by

$$X_i = \sum_{i=1}^{N_s} \alpha_{ij}[M_i] \tag{2.27}$$

where the α_{ij} is the third body efficiency. The rate of mass production Eq. 2.21 becomes,

$$\dot{R}_i = \sum_{j=1}^{N_r} \left(v_{ij}^{"} - v_{ij}^{'}\right) [X_i] \left\{ k_{f,j} \prod_{i=1}^{N_s} [M_i]^{v_{ij}^{"}} - k_{f,j} \prod_{i=1}^{N_s} [M_i]^{v_{ij}^{'}} \right\} \tag{2.28}$$

Chapter 3

NUMERICAL METHOD

In a chemically reacting flow there are several numerical difficulties that have to be taken into account. In a reactive flow the species continuity equations are coupled with the governing equations that have to be solved simultaneously. Due to a wide range of time scales in the flow, that leads to numerical stiffness that has to be compensated for and there is physical complexity due to coupling of fluid and chemical kinetics. In the case of detonation due to the discontinuity and small-time steps, an extremely fine grid spacing is required to model the discontinuity across the detonation.

3.1 Density-based solver

In the governing equations as the flow and chemical kinetics are coupled with each other they have to be solved simultaneously. The density-based solver solves the governing equation of continuity, momentum, energy and species transport simultaneously in a coupled manner as in the flowchart described in Fig. 3.1. Since the governing equations are nonlinear, several iterations of the solution loops have to be performed before obtaining the converged solution [12][13].

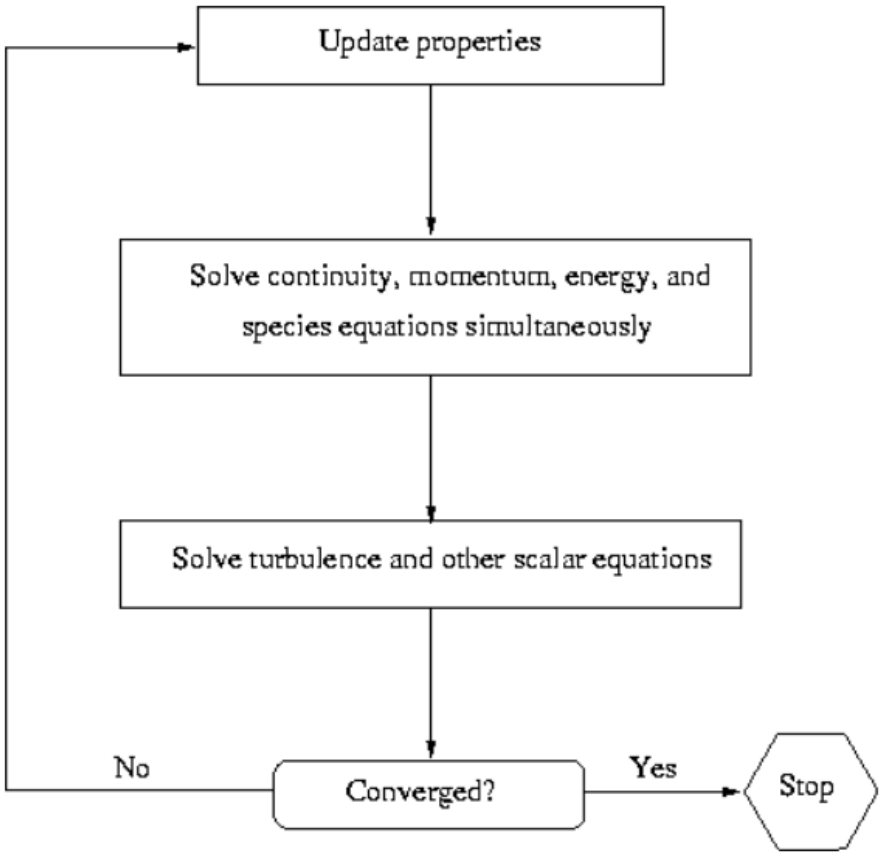

Fig 3.1: Solution method in a density-based solver

The density-based solver discretizes the non-linear equation into a linearized form to have a system of equations for a dependent variable in each cell. The resulting linear variables can be solved by two methods, explicit and implicit. In this case, the density based implicit solver is chosen. In the implicit solver, the governing equations are linearized implicitly with respect to all the dependent variables in the set. This results in a linear system of equation with ***N*** equations for each cell in the

domain that has to be solved simultaneously, where $\boldsymbol{N}$ is the number of coupled equations in the governing set of equations. For example, in terms of continuity, momentum in x-direction and y-direction, and energy, the unknowns are p, u, v, and T. By simultaneously solving the unknowns using a block Algebraic Multi-Grid (AMG) solver, this gives an implicit approach to solve the unknown variables at the same time.

3.2 Discretization and Solution

A finite volume formulation was used to convert the transport properties to an algebraic form in the two-dimensional reactive Euler equation given in Eq. 2.1, which is expressed as follows,

$$\int_V Q\, dV + \oint \mu.\phi\, dA = \int_V S\, dV \tag{3.1}$$

where V is the control volume, A is the surface area, μ is flux term defined as

$$\mu = F\hat{\imath} + G\hat{\jmath} \tag{3.2}$$

and ϕ is the normal unit vector defined as $\mu = dx\hat{\imath} + dr\hat{\jmath}$

3.3 Spatial Discretization

Monotone upstream – centered schemes (MUSCL): In order to achieve third order accuracy in space the MUSCL scheme [21][18] was employed. The values at face υ_f are been interpolated from the cell center values. This is accomplished by using upwind schemes. The upwinding means the face values υ_f is derived from the quantities of the cell upstream in the direction normal to the velocity. Monotone upstream-centered schemes for conservation laws (MUSCL) were used for the flow spatial discretization. The MUSCL is a created by blending the central difference scheme and second-order upwind scheme. The formulation of the MUSCL scheme is given by

$$\upsilon_f = \Theta\upsilon_{f,CD} + (1-\Theta)\upsilon_{f,SO} \tag{3.3}$$

where $\upsilon_{f,CD}$ is obtained from the central difference scheme as follows,

$$\upsilon_{f,CD} = \frac{1}{2}(\upsilon_0 + \upsilon_1) + \frac{1}{2}\left(\nabla\upsilon_0.\ \phi_{0f} + \nabla\upsilon_1\ .\ \phi_{1f}\right) \tag{3.4}$$

where 0 and 1 terms represent the cell share faces. The ∇ terms are the reconstructed gradient at cell 0 and 1.

The term $\upsilon_{f,SO}$ is obtained from the second order upwind stream. The quantities at the cell faces are computed using multidimensional reconstruction approach [12][13][18] The higher order accuracy is achieved by Taylor series expansion of the cell centered solution. It is computed as follows,

$$\upsilon_{f,SO} = \upsilon + \nabla\upsilon \cdot \phi_f \tag{3.5}$$

where υ and $\nabla\upsilon$ are the cell center values and the gradient of the cell center values respectively in the upstream. ϕ represents the displacement vector from the upstream of the cell face centroid. The gradient term is spatially discretized by using second order upwind scheme, is the Green-Gauss cell-based which is discussed below.

Green-Gauss Theorem: The gradients used for computing values of a scalar term ϕ at the cell faces center.[21][18][20] The Green – Gauss theorem is described as

$$(\nabla\upsilon)_c = \frac{1}{v}\sum_f \phi_f \, A_f \tag{3.6}$$

where ϕ is referred as the gradient of the scalar properties at cell center c, and ϕ_f represents the value of ϕ at the cell face center is expressed as,

$$\phi_f = \frac{\phi_{c0} + \phi_{c1}}{2} \tag{3.7}$$

where ϕ_{c0} and ϕ_{c1} are the values at the neighboring cell centers.

Advection Upstream Splitting Method (AUSM): The convective fluxes at each cell F and G in Eq. (3.1) are approximated by the flux vector splitting scheme known as Advection upstream splitting method (AUSM). This was introduced by Liou and Steffen in 1993 [21][19][18]. This scheme first computes a cell interface Mach number based on the characteristic speed from the adjacent cell. The interface Mach number is then used to determine the upwind extrapolation for the convection part of the fluxes. The pressure terms are obtained by splitting of Mach number. A generalized Mach number-based convection and pressure terms were proposed by Lion [21[19][18]. This provides the resolution for the shock discontinuity and damps the oscillations at stationary and moving shocks. The scheme is expressed as follows,

$$F = m_f v + P_i \tag{3.8}$$

where m_f represents the mass flux through the interface. The mass flux is calculated from left to right of the interface by using the forth order polynomial.

Temporal discretization: For a transient simulation, the governing equations Eq. (2.1) and Eq. (2.2) must be discretized in both space and time. This involves the discretization of the terms at every time step Δt. The generic expression for the scalar quantities with respect to time step is given by

$$\frac{\delta v}{\delta t} = F(v) \tag{3.9}$$

The time derivative was calculated using a backward difference, second-order discretization is expressed as

$$F(v) = \frac{3v^{i+1} - 4v^{i} + v^{i-1}}{2\Delta t} \tag{3.10}$$

where υ is the scalar quantity, i is the value at the current time step, i+1 is the value at t + Δt and i-1 is the value at t – Δt.

An implicit time integral was selected, because the scheme is unconditionally stable with respect to time step size. The downside of an implicit scheme is, if the solver was not optimized then the runtime will increase drastically. The formulation to evaluate $F(\upsilon^{i+1})$ is given by,

$$\frac{v^{i+1} - v^{i}}{\Delta t} = F(v^{i+1}) \tag{3.11}$$

where

$$v^{i+1} = v^{i} + \Delta F(v^{i+1}) \tag{3.12}$$

High order term relaxation: The importance of high order terms is to improve the start-up and the general solution behavior of flow simulations when a higher

order spatial discretization's were used. This also prevents convergence stalling, in many cases which leads to numerical instabilities. The HOTR is used to reduce the interaction of numerical instabilities in an aggressive solution. The HOTR is written as the first order scheme plus the additional terms from the higher order schemes. The Relaxation factor for the higher order scheme is described as follows,

$$\varphi_{i+1} = \varphi_i + f(\varphi_{i+0.5} - \varphi_i) \tag{3.13}$$

where, φ is a generic formulation for any terms from single to higher order, and f is the under-relaxation term.

Algebraic Multigrid (AMG): In this case a F – cycle multigrid was selected. F-cycle is essentially a combination of V and W cycles as described below in Fig 3.2

$$\boldsymbol{pre\ sweep \rightarrow restrict \rightarrow W\ cycle \rightarrow V\ cycle \rightarrow prolongate \rightarrow post\ sweep}$$

Fig 3.2: F – cycle multigrid solver

where the restriction and propagation are used based on the additive correction strategy [21][18].

3.4 Boundary Conditions

Pressure Inlet: In the case of a compressible inlet the pressure inlet evaluates the isentropic flow relations using ideal gas relations. The input, total pressure P_0 and the static pressure P_s in the adjacent cells are related as,

$$\frac{P_0 + P_{op}}{P_s + P_{op}} = \left(1 + \frac{\gamma - 1}{2} M^2\right)^{\frac{\gamma}{\gamma - 1}} \tag{3.14}$$

where

$$M = \frac{V}{\sqrt{\gamma R T_s}} \tag{3.15}$$

The density and the temperature at the inlet plane is from the ideal gas law that is given as follows,

$$\rho = \frac{P_s + P_{op}}{R T_s} \tag{3.16}$$

$$\frac{T_0}{T_s} = 1 + \frac{\gamma - 1}{2} M^2 \tag{3.17}$$

where op is the operating condition. The individual velocity components at the inlet are derived using the direction vector components.

Pressure Outlet: This outlet condition extrapolates the values at the exit from the interior of the domain. The extrapolation is carried out by using the splitting procedure based on the AUSM scheme [4][18][20][21].

Symmetry: The geometry is taken to be 2-D axis-symmetric. There are no flux terms across the boundary with zero normal velocity component.

3.5 Computational Resources

Generally, a chemically reactive flow solution requires an extended amount of computational time and resources are required in order to obtain a converged and accurate solution due to the complexity in the problem. The run-time of the numerical simulation of a reactive flow is reduced by using multiple CPU's with optimum number of cores and nodes. Extensively increasing the processor number will also lead to increase in run-time, as the commutation time among the processor cores are higher than the communication between the nodes, for an efficient performance minimum communication among the processors has to be maintained. Stampede 2 from Texas Advanced Computing Center (TACC) [22][23] was utilized remotely for running the simulations. The TACC was accessed through windows secured copy (WinSCP) protocol. The flowchart in Fig 3.3 represents the process involved in accessing fluent in TACC.

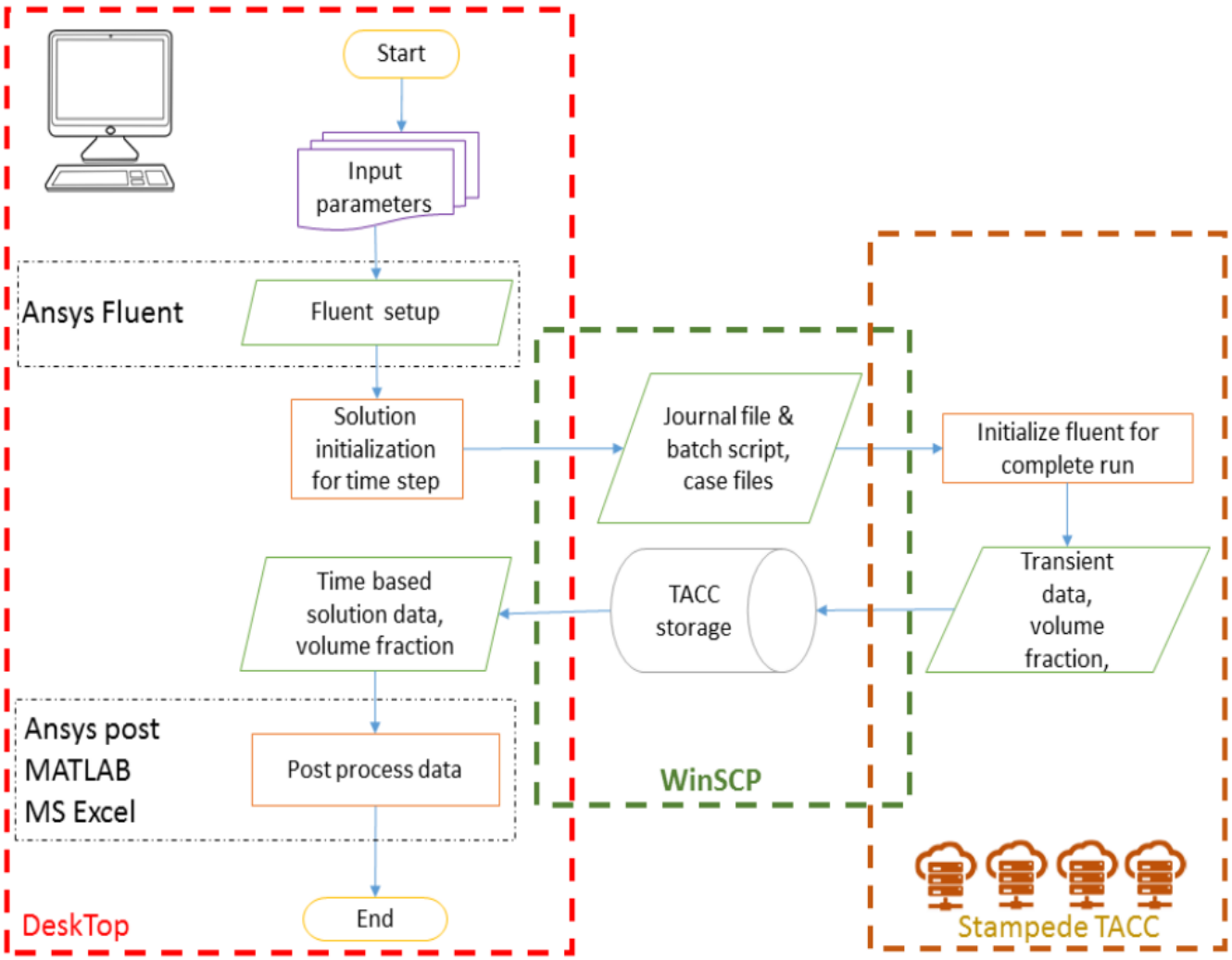

Fig 3.3: Accessing Fluent in TACC

Chapter 4

CHEMISTRY MODELING

The stability of the chemical reaction plays a vital role in the detonation combustion. In order to model the chemical kinetics, chemked was used which runs Chemkin III solver in the background. The results obtained from chemked is validated by comparing with the NASA CEA results [12][13][10].

The formulas used to calculate the reaction rate is explained in section 2.3. The input file for the Chemked is in the Chemkin III format [10] and was modified according to the required case. The input file for the chemical kinetics solution for the detonation in Chemkin format is provided in the APPENDIX, along with the thermodynamic properties of the materials in the reaction which was obtained from NASA-CEA [12] and GRI mech [13][10]

The rate change of mole fraction with respect to time is compared with T.H.Yi [20] and Chemkin III: A Fortran chemical kinetics package for analysis of gas-phase chemical and plasma kinetics [10], with the following initial conditions of, pressure as 1 atm, and temperature as 1500 K. The initial mole fraction of hydrogen is 0.296, oxygen is 0.148, nitrogen is 0.556 which corresponds to the stoichiometry for

hydrogen-air reaction [4][6][20]. The hydrogen-air reaction mechanism considered here is a 11 species and 23-step reaction model which has an operating range from 400 K to 6000 K. This reaction takes into consideration of all the quantum modes of energy in the molecule, as the vibrational mode tends to dominate above 2800 K for Nitrogen molecule, which is near to the detonation temperature of hydrogen-air for the given operating condition.

Increasing the number of chemical steps in the model, will provide a detailed separation of the induction and reaction zone in the detonation. But while considering the global scale of the problem, the complexity of the solution will increase which in turns increases the runtime of the simulation. So, compromises had to be made in selecting an appropriate reaction model for the hydrogen-air reaction without losing the details that are required for simulating a detonation. For the above mentioned initial condition, the Fig 4.1 provides the rate change of mole fraction of the species with respect to time. The graph was generated using MatLab from the data that been obtained from the Chemked solver.

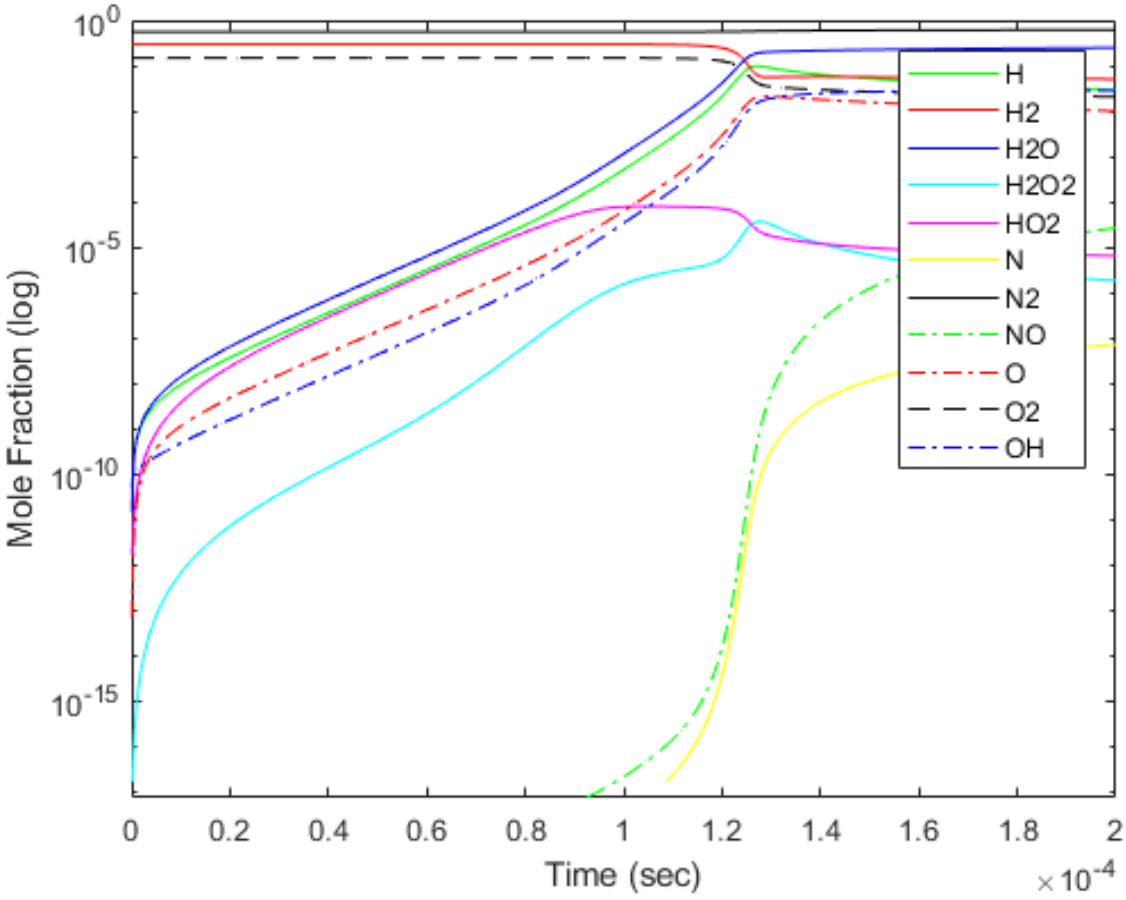

Fig 4.1: Time variation of mole fraction for 23 step and 11 species hydrogen -air reaction p = 1 atm and T = 1500 K

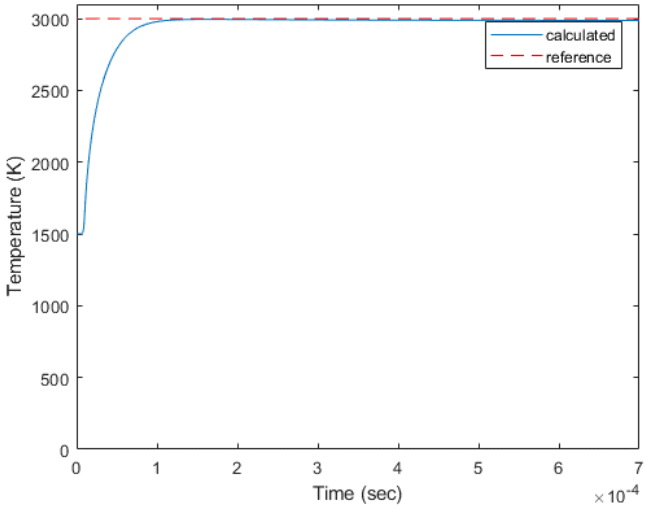

Fig 4.2: Temperature variation with respect to time

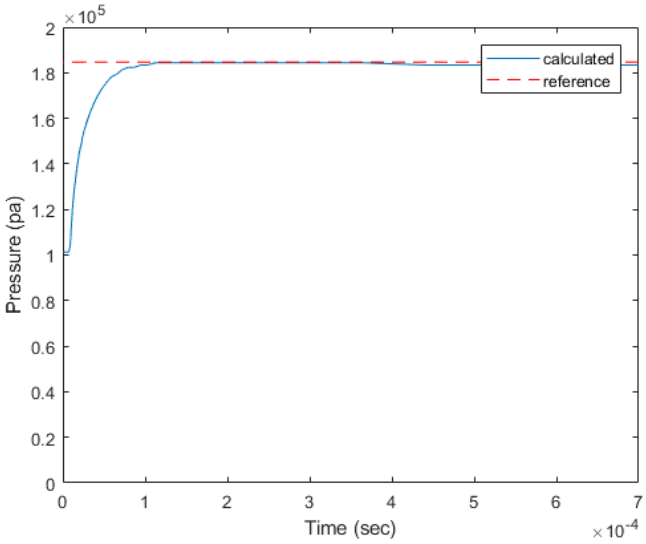

Fig 4.3: Pressure variation with respect to time

Chapter 5

GEOMETRY AND GRID STUDY

In this chapter, we discuss about the geometry and the grid study of the 2-D axisymmetric combustion chamber for unsteady detonation-simulation. And also, the methods that are used to validate the boundary condition in order to obtain the required results in a cold flow and the necessary steps that have been carried out for a grid independence study for the given geometry to capture the detonation C-J condition by checking the pre and post-shock properties, along with the C-J condition the NASA CEA [12][13].

The combustor geometry is a two-dimensional axis-symmetric combustion chamber consisting of a wedge followed by a shock cancelation zone. The wedge angle was chosen after a flow study carried out on different wedge angles for different modes of detonation done by Hui – Yuan Fan [6][4][20]. The wedge angle of 15^{o} is selected because this lies in a complex region where the initiation of both oblique and normal detonation wave is made possible by changing the inlet condition of the combustion chamber. The sketch of the geometry is given in Fig 5.1.

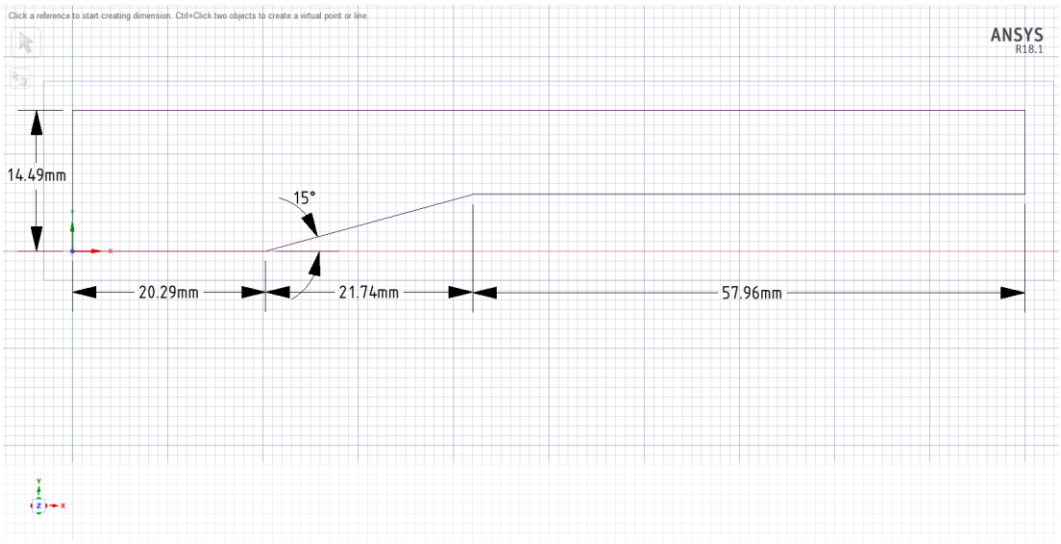

Fig 5.1: Two – Dimensional combustion chamber

SOD shock tube problem: This problem is being taken as a base reference in order to check if the given initial conditions and the solver for the given geometry with the following structured grid size are able to capture the shock along with the pre and post-shock conditions. The geometry used for the SOD problem with the grid used is displayed in Fig 5.2. The initial condition of the region 4 and region 1 in the shock tube are given as follows,

$$(\rho, v, p) = \begin{cases} (1.0, 0, 1.0) & if \quad 0 < x < 5 \\ (0.125, 0, 0.1) & if \ 5 < x < \ 10 \end{cases} \tag{5.1}$$

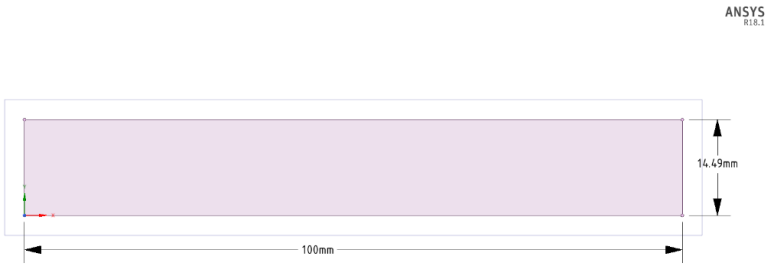

Fig 5.2: SOD Shock tube problem (SOD) geometry

The plots in Fig (5.3), (5.4), (5.5) represents the ρ,υ, p at a given time are expressed in a was it been expected. From this it can be inferred that the given geometry with the following grid size of 0.09 mm with a time step of 10^{-5} sec is capable of capturing the shock with the above-mentioned boundary condition.

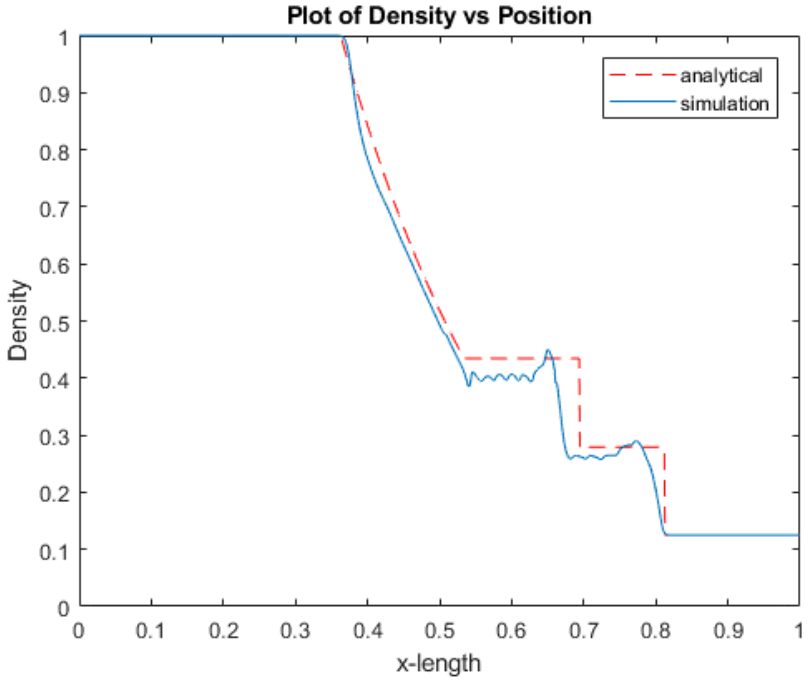

Fig 5.3: Density along x-axis

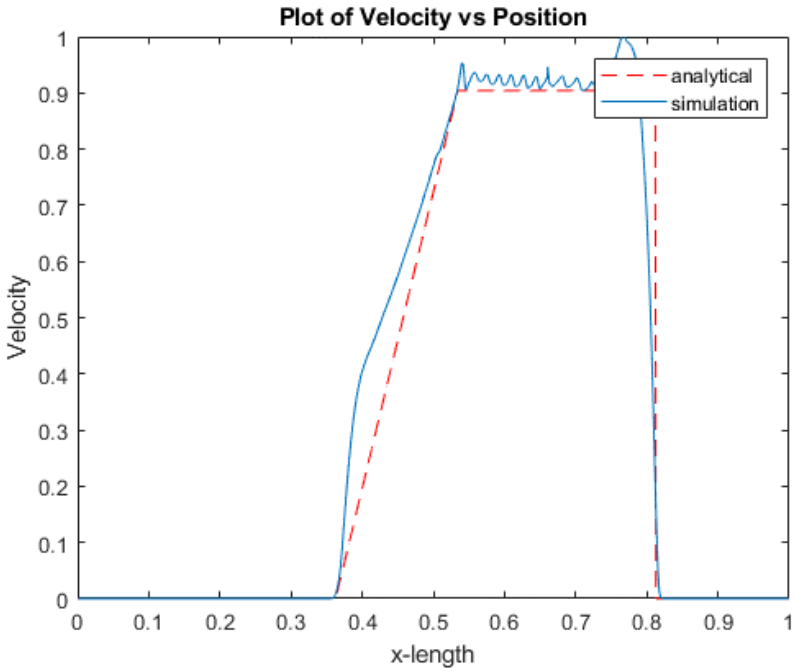

Fig 5.4: velocity along x-axis

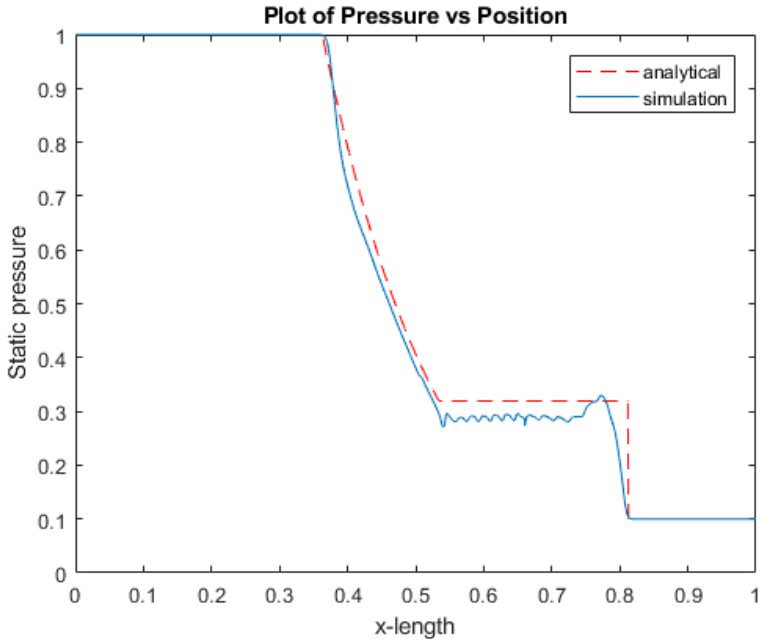

Fig 5.5: pressure along x-axis

Grid independence study: The grid independence study is important for modeling a detonation, as the detonation wave speed is strongly dependent on the grid spacing [6][20]and this also helps in analyzing an appropriate grid size, so the detonation is not inadequately resolved which leads to divergence and improper results, or highly resolved which increases the total time, but with just 1% or 2% variations in the required output. For the grid independence study, a model which measures 10 x 1.449 cm^2 in length and height was created with a grid sizing of 0.1, 0.09, 0.07, 0.03 mm. The entire geometry was initialized with the stoichiometric hydrogen-air mixture with was solved by the chemical kinetics that has been discussed in chapter 4 with the pressure of 1 atm and temperature of 700 K. The CJ conditions and detonation parameters for stoichiometric hydrogen-air mixture at the given initial condition is obtained from NASA-CEA which are, $\frac{p}{p_1}$ is 6.631 and $\frac{T}{T_1}$ is 4.291. p and T are the post-detonation pressure and temperature, were p equates to 671900 pa and T equates to 3003.47 K [12][13]. To initiate detonation in the tube a high enthalpy region of pressure 40 atm and temperature 4000 K was patched at the closed end of the tube that has been shown in Fig 5.6 and the other end is set to be a pressure outlet to atmosphere condition. The Fig 5.7, 5.8, 5.9 are the graph comparison for pressure, temperature, and velocity respectively at a given time $5.2x10^{-4}$ seconds. It can be seen that grid size plays an important role in achieving CJ condition for the given condition and chemical reaction. As it can be observed

from the Fig (5.7)(5.8) grid size 0.03 mm is the preferred grid size for capturing the detonation.

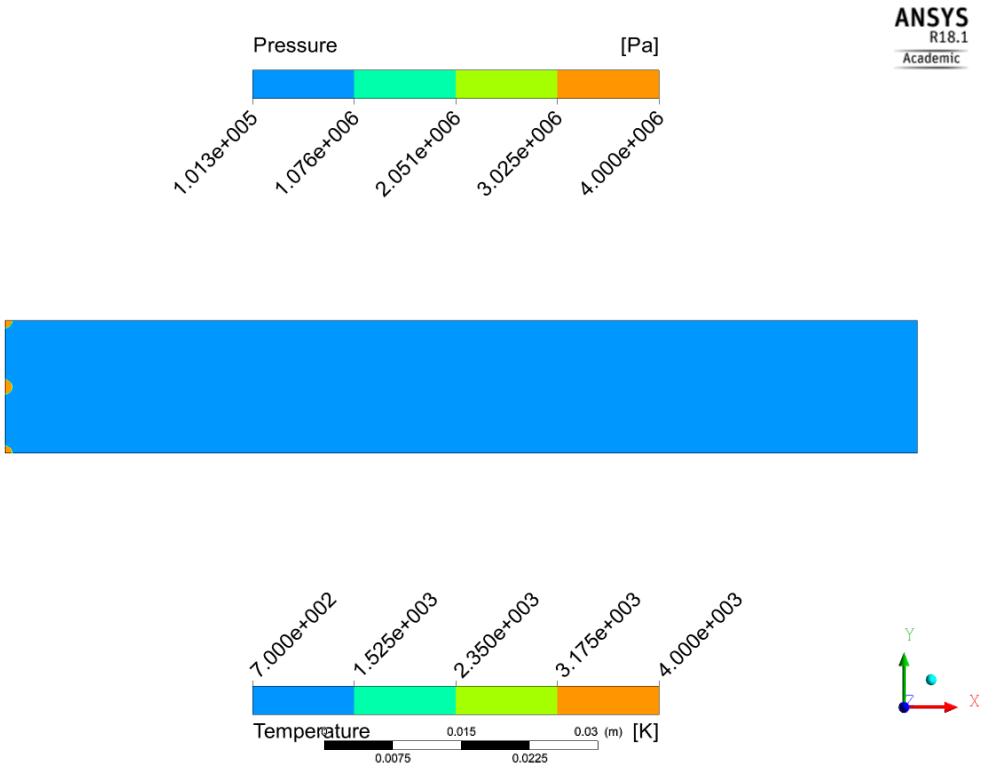

Fig 5.6: Initial pressure and temperature contour for grid study

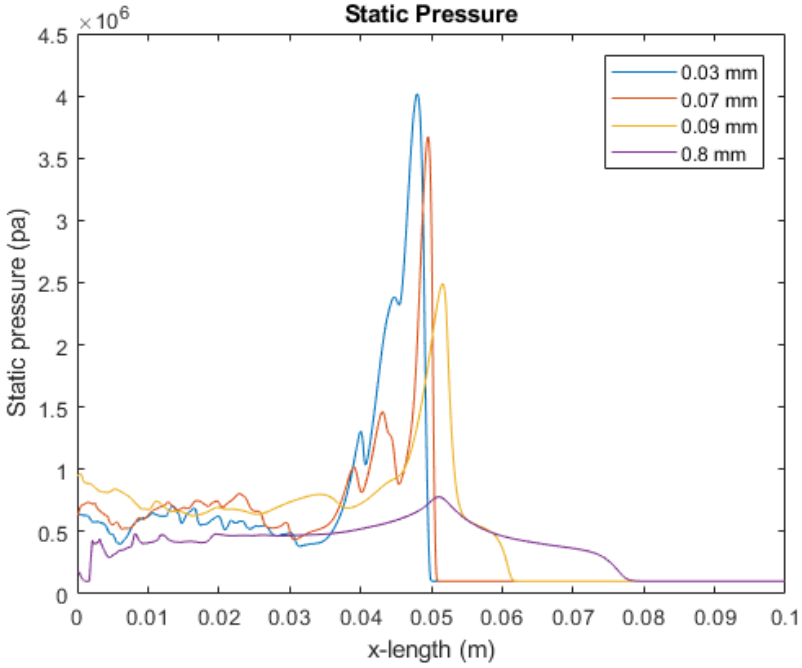

Fig 5.7: Pressure along x-axis at time 4.5 x 10^{-4} sec

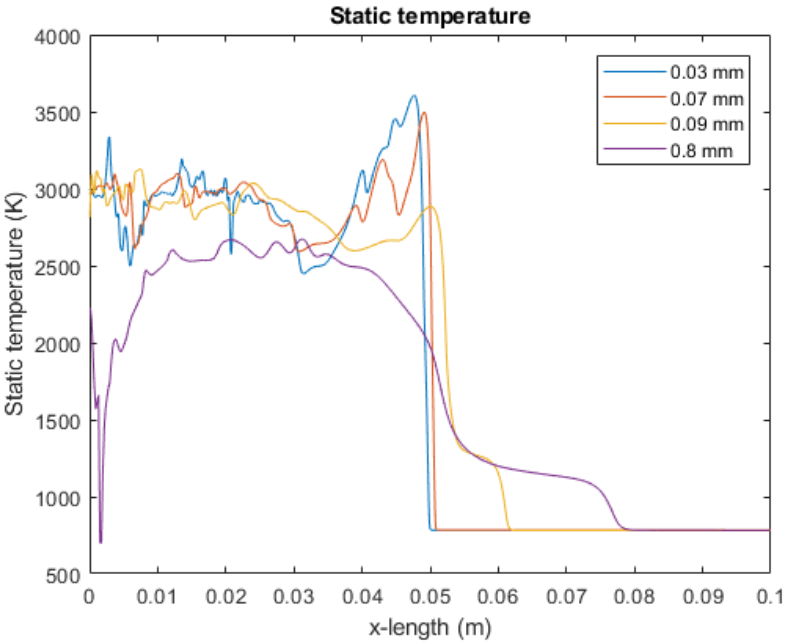

Fig 5.8: Temperature along x-axis at time 4.5 x 10^{-4} sec

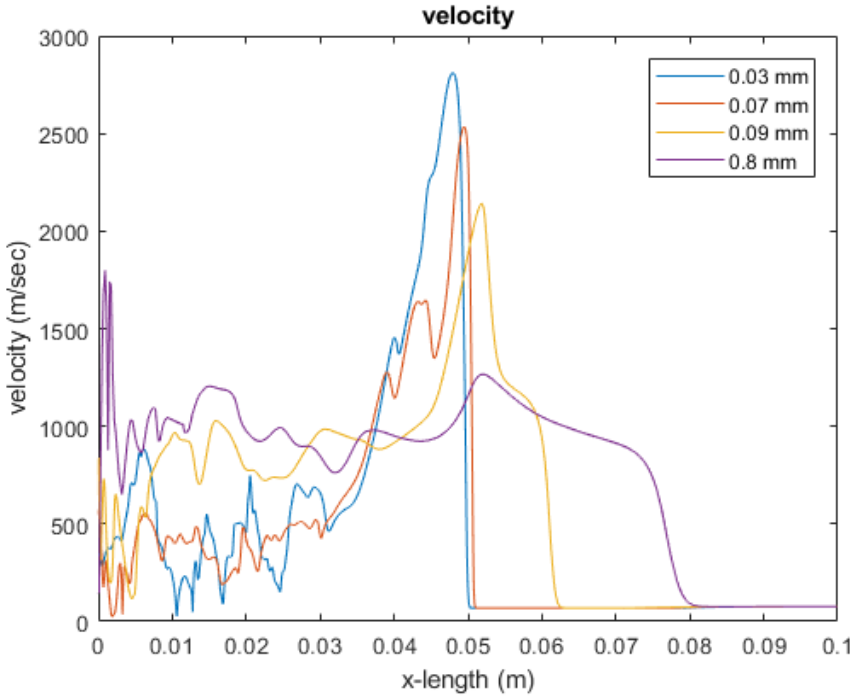

Fig 5.9: velocity along x-axis at time 4.5 x 10^{-4} sec

The fluctuations of values in the Fig 5.7 – 5.9 are due to the interaction of shear layer after the detonation cell that is visible in the Fig 5.11 – 5.13. the oscillations in the values can be reduced by reducing the grid size or by using an Adaptive Mesh Refinement (AMR).

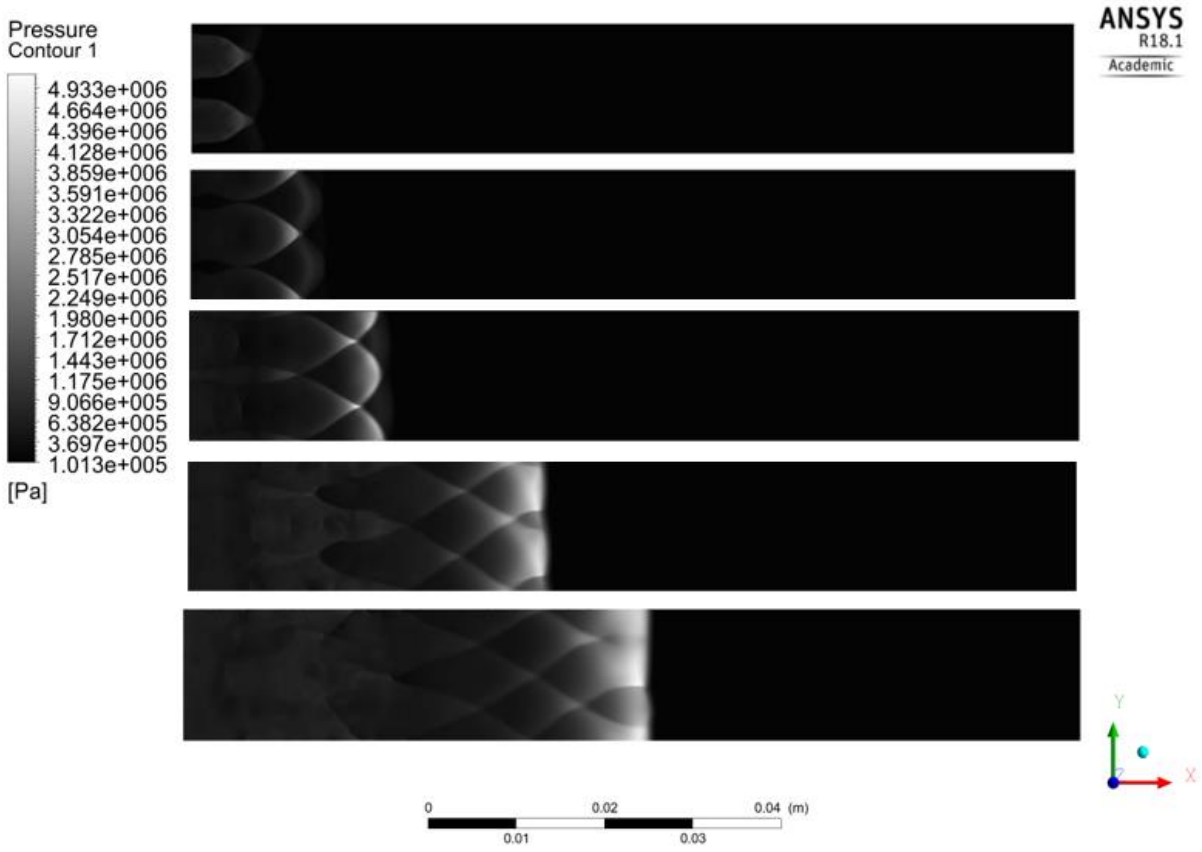

Fig 5.10: Detonation propagation in the grid size $0.03x10^{-5}$ m

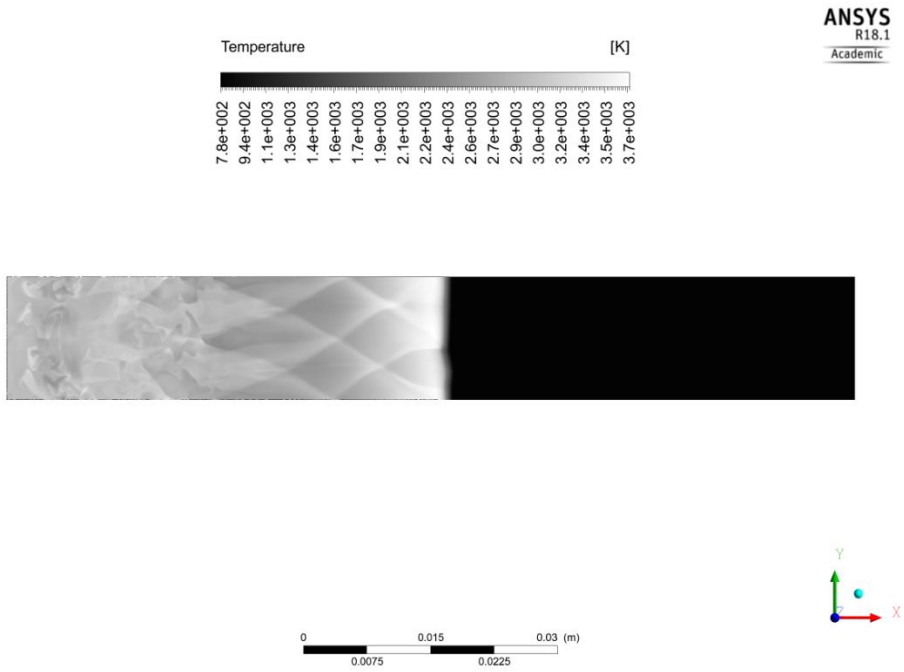

Fig 5.11: Temperature contour in grid size 0.03 m x10^{-5} m

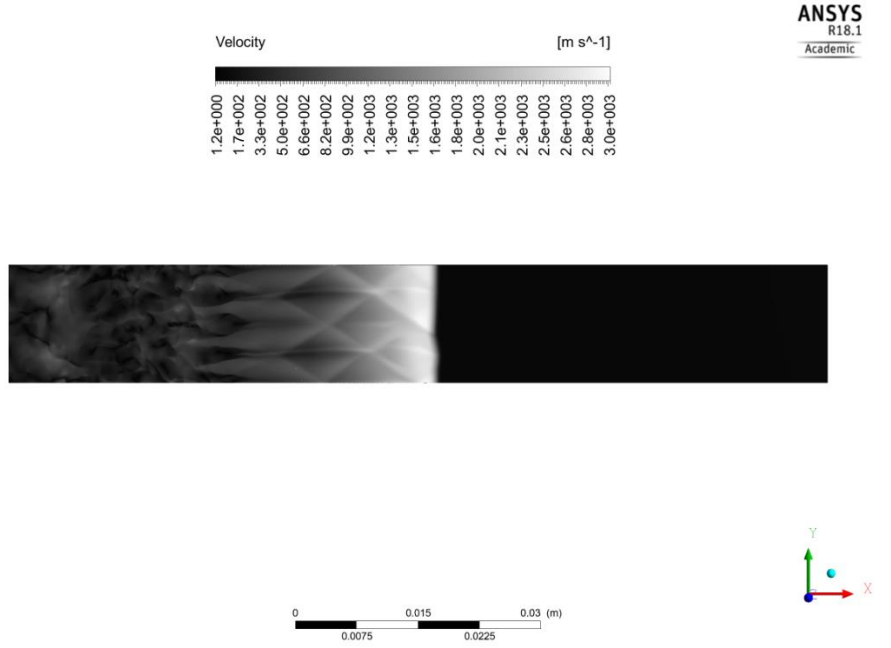

Fig 5.12: Velocity contour in grid size 0.03 x10^{-5} m

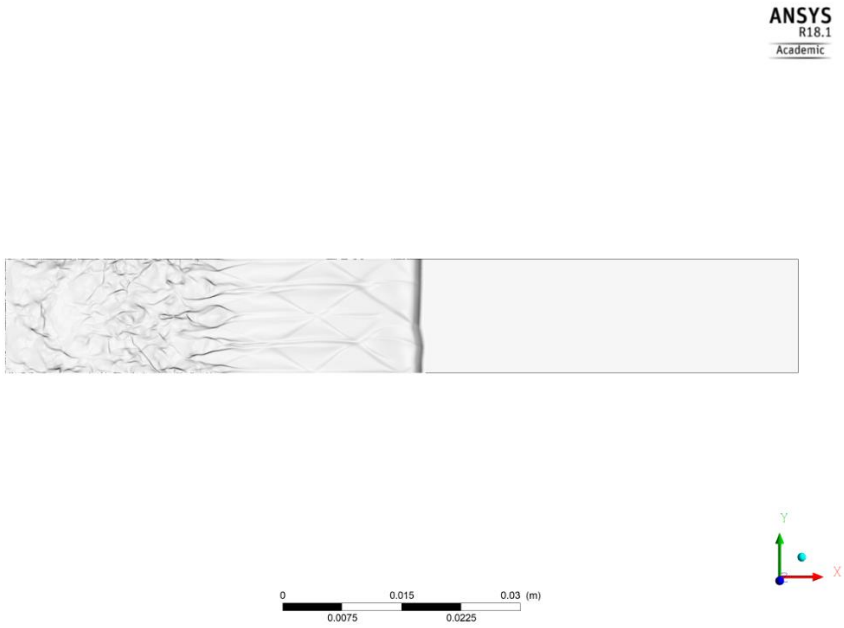

Fig 5.13: Numerical schlieren imaging

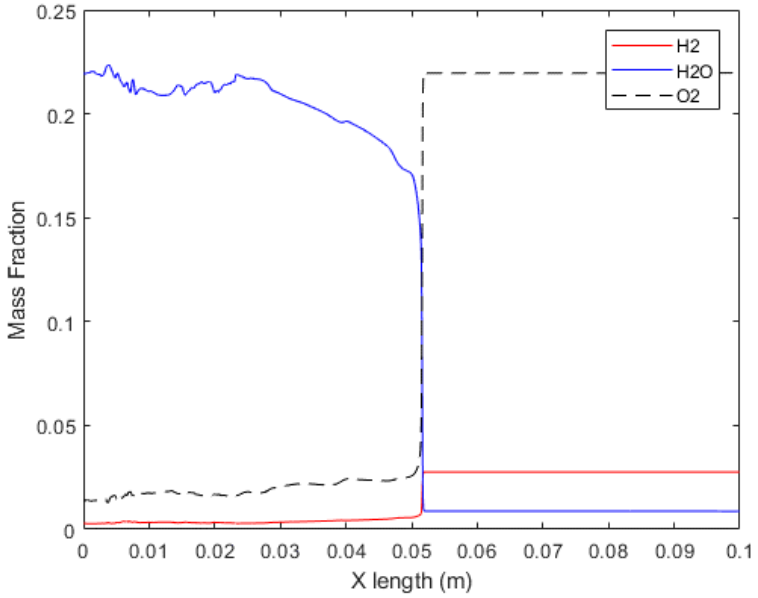

Fig 5.14: Mass fraction of H_2, O_2, H_2O

The Fig (5,10), (5.11), (5.12), (5.14) are the representation of pressure, temperature, velocity, heat of reaction and mass fraction of species (H_2 , O_2 , H_2O) respectively for geometry with the grid size of 0.03 mm. The Fig 5.1 represents the combustion chamber which was meshed with a grid sizing of 0.03×10^{-5} m. The total number of cells is 2,458,464 and nodes is 2,462,005. The schematic of a two-dimensional combustion chamber has been described in the Fig 5.1.

Chapter 6

RESULTS AND DISCUSSION

The results were analyzed and post-processed using ANSYS CFD-Post [18][20][22] and the numerical schlieren was created by using paraview. In a simulation of unsteady normal detonation, the concept of detonation strength had to be understood properly. As its known that if the detonation incoming Mach number ($M_{3.5}$) is less than the CJ Mach number (M_{CJ}) for the given stoichiometry condition the detonation wave tends to move upstream in the combustion chamber, and on the other hand if the detonation incoming Mach number ($M_{3.5}$) is higher than the CJ Mach number (M_{CJ}) for the given stoichiometry condition then the detonation tends to move downstream along with the flow [4][6][15]. The above property of detonation was utilized in order to move the detonation wave upstream and downstream inside the combustion chamber. As the detonation strength depends on the detonation chamber incoming Mach (M_3), the M_3 is varied by fixing the flow inlet properties namely the pressure, temperature, and velocity to a particular value in a cycle, and varying the mass fraction of the fuel.

For the case - I the M_{CJ} equals to 3.108 for a stoichiometric hydrogen-air with pressure 101325 Pa and temperature 700 K as initial condition. The combustion chamber incoming Mach number 3.5 will have $M_{3.5}$ equivalent to 2.669, due to the

presence of oblique shock formed by the wedge. With $M_{3.5}$ being less that M_{CJ} the detonation wave would propagate upstream. If the fuel is turned off that would make the incoming flow to purge the combustion chamber and would convert the propagating detonation wave to a propagating blast wave. This blast wave will eventually die off with no fuel in the incoming flow. The problem faced in this scenario was the length required by the blast wave to reduce in strength and die off was longer than the length anticipated, which was solved by changing the incoming flow equivalence ratio to 0.5 instead of purging the chamber. The M_{CJ} equals to 2.82 for an equivalence ratio of 0.5 with the same initial conditions. The change in γ makes the combustion chamber incoming Mach number to 3.8, that with have a $M_{3.5}$ equal to 2.91. The M_3 being larger than M_{CJ} the detonation wave will propagate downstream with the flow. This method of NDW will oscillate the detonation wave inside the combustion chamber and will produce a constant flow properties at the combustion exit plain.

Flow of this chapter is going to be as follows, first explaining the different cases for an unsteady normal detonation wave combustion, which provides the cycle time. The cases are varied according to their initial conditions variables namely pressure, temperature, and velocity. The final part of the chapter is to analyze the variation in pressure, temperature and velocity ratios with respect to time at the exit

of the combustion chamber. The Table 6.1, 6.2, 6.3 consists of the initial conditions for the different cases.

	Equivalence ratio	Inlet condition	Time steps	elapsed time (sec)
Case I	Equivalence ratio - 1	Pressure – 101325 pa Temperature – 800 K Mach number – 3.5 Velocity – 2304.874 m/sec	0 to 1500	1.5×10^{-4}
	Equivalence ratio – 0.5	Pressure – 101325 pa Temperature – 800 K Mach number – 3.8 Velocity – 2303.281 m/sec	1500 to 7000	5.5×10^{-4}
	Equivalence ratio – 1	Pressure – 101325 pa Temperature – 800 K Mach number – 3.5 Velocity – 2304.874 m/sec	7000 to 8000	1×10^{-4}
	Equivalence ratio – 0.5	Pressure – 101325 pa Temperature – 800 K Mach number – 3.8 Velocity – 2303.281 m/sec	8000 to 11500	3.5×10^{-4}
	Equivalence ratio - 1	Pressure – 101325 pa Temperature – 800 K Mach number – 3.5 Velocity – 2304.874 m/sec	11500 to 12500	1×10^{-4}

Table 6.1: case I

CASE I: In this case, as mentioned in Table 6.1 the initial conditions are, static pressure in the combustion chamber is 101325 Pa, the static temperature is 800 K with a Mach number of 3.5 that gives the velocity in x-axis at the inlet to be 2304 m/sec, the equivalence ratio for this cycle φ is 1. It is necessary to have a similar flow time step and chemical time step in order to avoid the instabilities. This requires the flow to have a time step of a 10^{-7} sec, which is the appropriate time step for a detonation with the specified chemical kinetics of hydrogen-air [2][20][6]. In this case, the M_3 is less than the M_{CJ} which causes the detonation to propagate upstream. The detonation should be made to move downstream before it crosses the wedge because, if the detonation is upstream of the wedge, due to the presence of a strong normal shock in front of the reaction zone, which in turn causes the detonation to propagate upstream no matter what the inlet equivalence ratio is set. The next cycle starts when the equivalence ratio φ is changed to 0.5, while maintaining the same inlet pressure, temperature and velocity. This causes the Mach number to go up to 3.8, which makes the M_3 to be higher than M_{CJ}. A single cycle time is the addition of first and second stage elapsed time. The evolution of the flow from initiation and propagation of an unsteady detonation wave with respect to time is shown in the Fig 6.1 – 6.5.

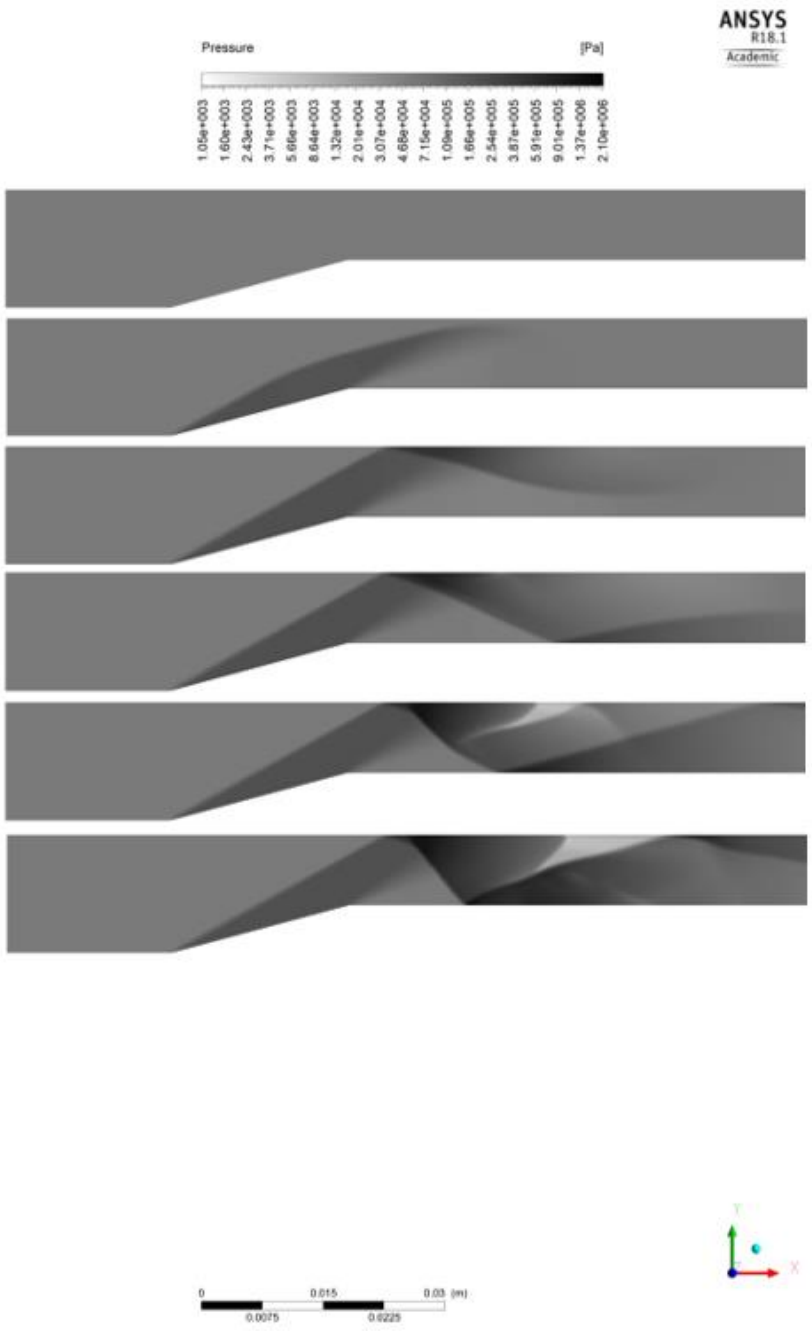

Fig 6.1: Time from 0 to 1.5 x 10^{-4}sec

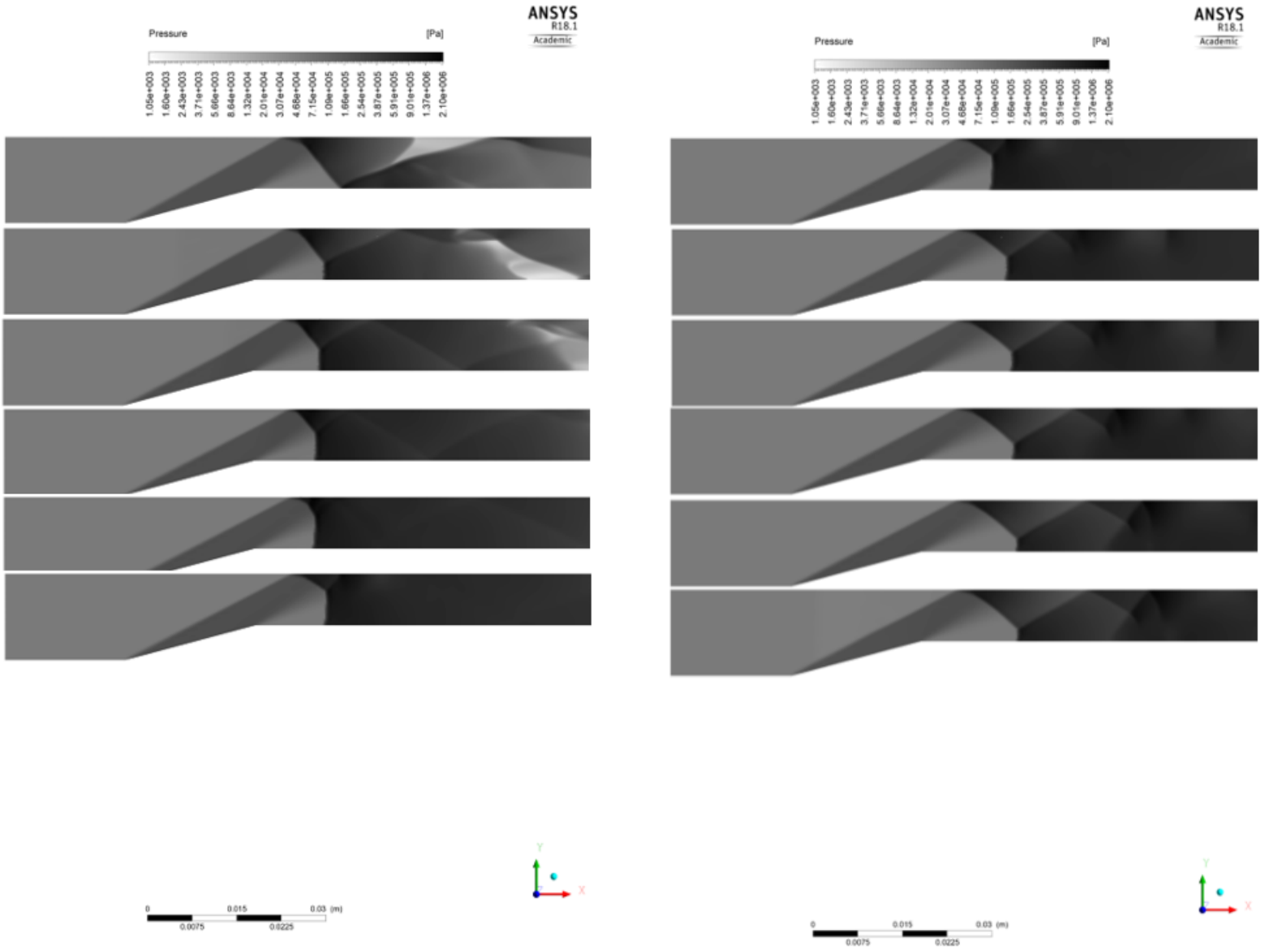

Fig 6.2 (a,b): Time from 1.5 x $10^{-4}$to 6.0 x 10^{-4}sec

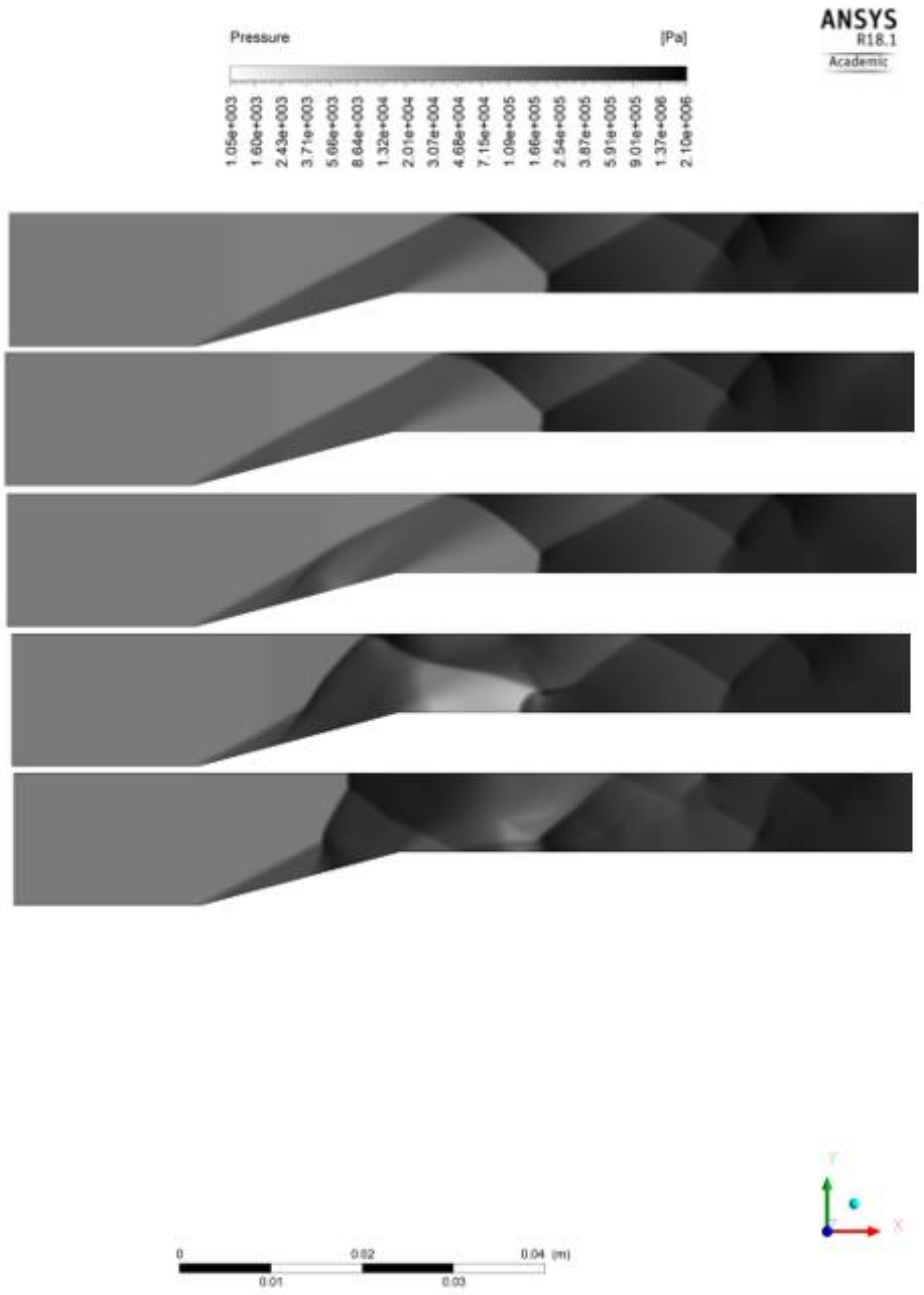

Fig 6.3: Time from 6.0 x 10^{-4} to 7.0 x 10^{-4} sec

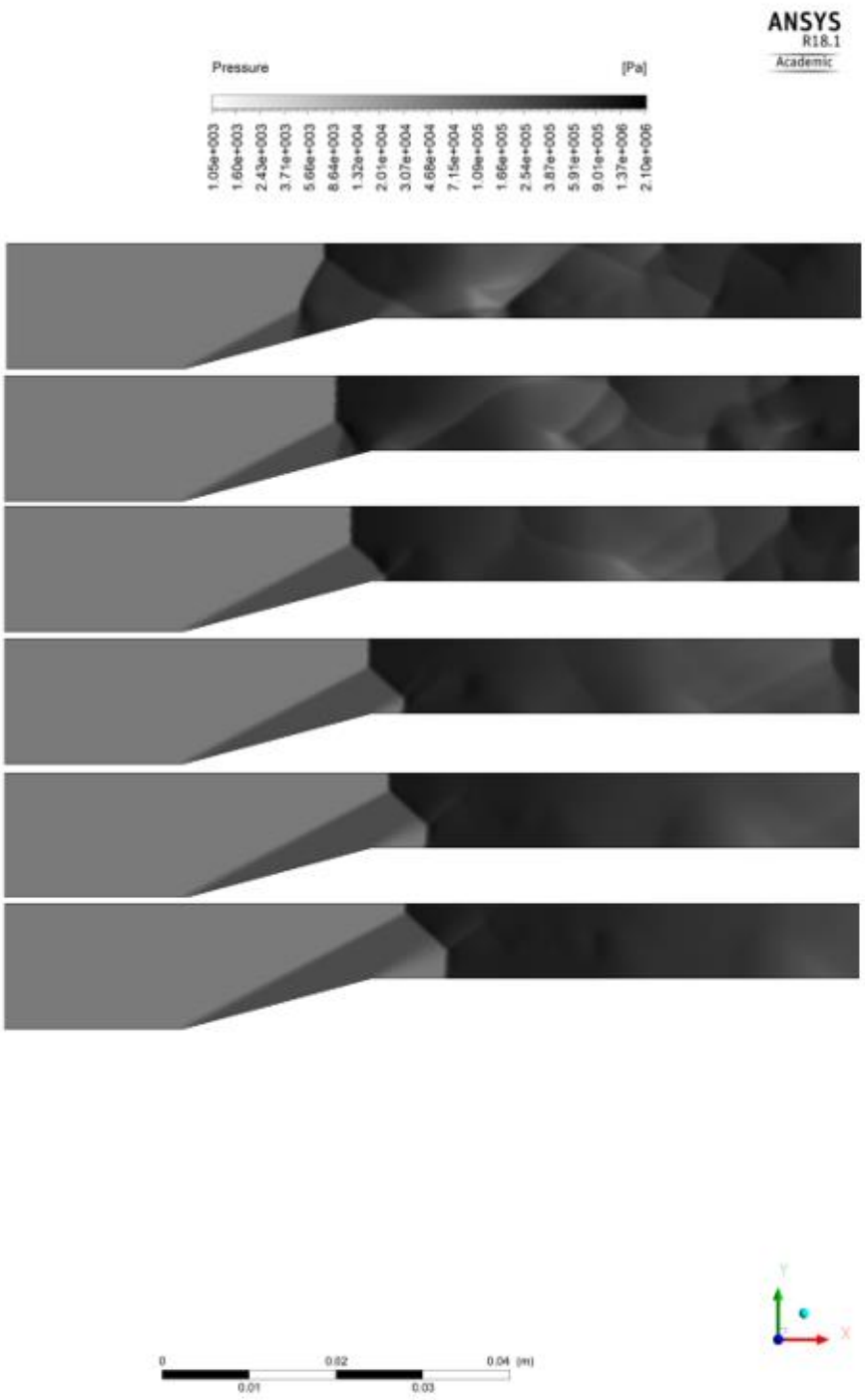

Fig 6.4: Time from 7.0 x 10^{-4} to 1.4 x 10^{-4}sec

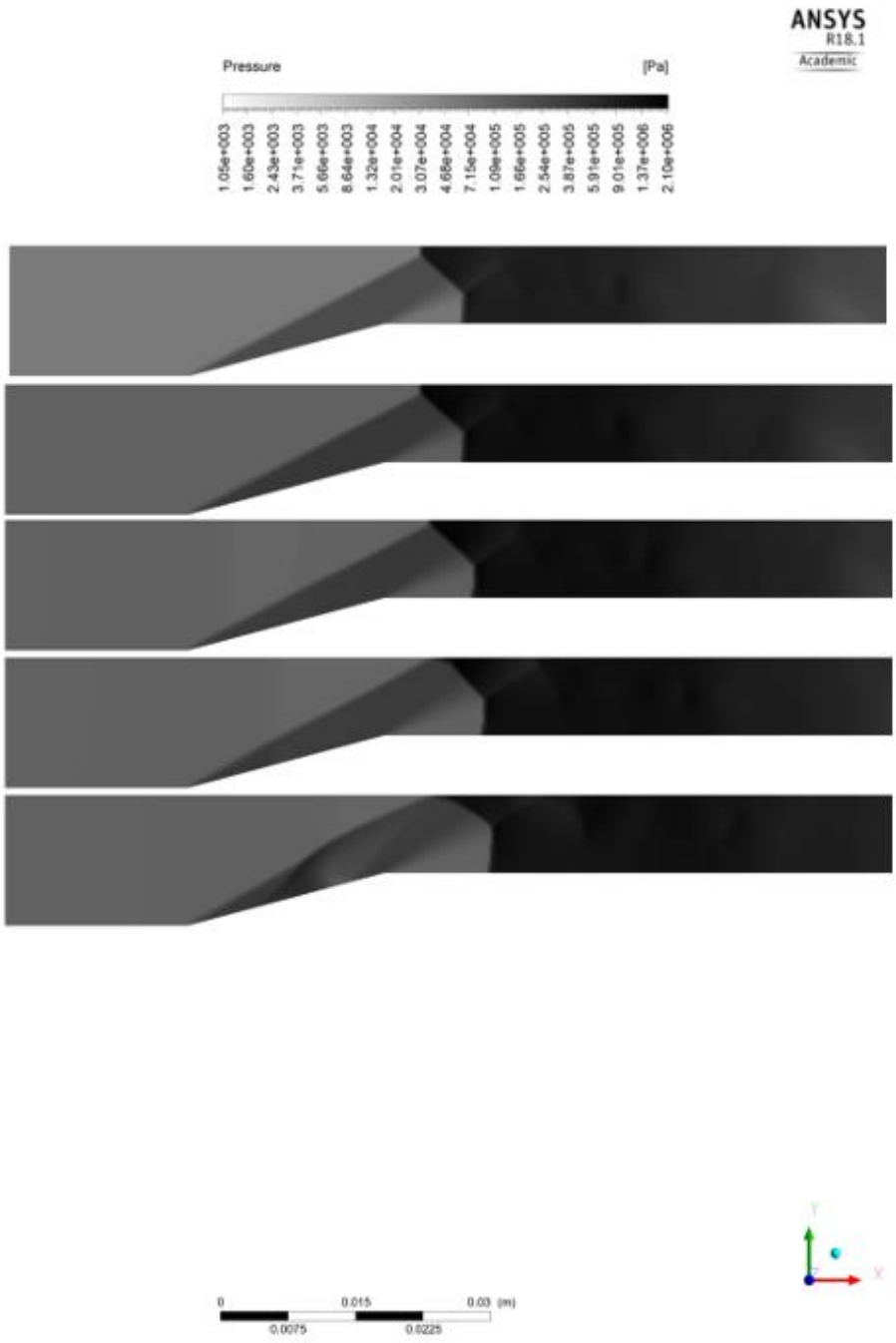

Fig 6.5: Time from 1.4 x 10^{-4} to 2.4 x 10^{-4} sec

CASE II: The initial conditions and the cycle time is mentioned in Table 6.2. The methodology is similar to the CASE 1, but the difference is in the initial conditions. The initial conditions for this case are, a static pressure in the combustion chamber of 50662.5 Pa which corresponds to a high-altitude flight, with a static temperature of 800 K, Mach number of 3.5 with an equivalence ratio of 1. This equates to a flow velocity at the combustor inlet of 2304 m/sec. The second cycle of this case starts when the equivalence ratio is reduced to 0.5 and the pressure, temperature and velocity are maintained at the same values, which increases the flow Mach number to 3.79. The propagation of the flow is similar to that of the case I with minor variation in the cycle time**.**

	Equivalence ratio	Inlet condition	Time steps	elapsed time (sec)
Case II	Equivalence ratio - 1	Pressure – 50662.5 pa Temperature – 800 K Mach number – 3.5 Velocity – 2304.874 m/sec	0 to 4000	4×10^{-4}
	Equivalence ratio – 0.5	Pressure – 50662.5 pa Temperature – 800 K Mach number – 3.8 Velocity – 2303.874 m/sec	4000 to 5800	1.8×10^{-4}
	Equivalence ratio – 1	Pressure – 50662.5 pa Temperature – 800 K Mach number – 3.5 Velocity – 2304.874 m/sec	5800 to 8650	2.9×10^{-4}
	Equivalence ratio – 0.5	Pressure – 50662.5 pa Temperature – 800 K Mach number – 3.8 Velocity – 2303.874 m/sec	8650 to 10400	1.75×10^{-4}

Table 6.2: Case II

CASE III: The initial conditions and the cycle time are mentioned in Table 6.3. The methodology is similar to the above cases; the difference is in the initial conditions. The initial condition of this case is static pressure in the combustion chamber is 50662.5 pa which represents a high-altitude combustion. With a temperature of 700 K, flow Mach number of 3.5 and an equivalence ratio of 1. This equates the flow velocity at the combustor chamber inlet to be 2163 m/sec. The second cycle of this case starts when the equivalence ratio is reduced to 0.5, and with the pressure, temperature and velocity maintained at the same value, this increases the flow Mach number to 3.77. The propagation of the flow is different in this case when compared to the case I and case II, because in this case the enthalpy is lower than the previous cases. This causes the detonation to be initiated at the downstream from the wedge. The propagation of the flow for two continuous cycles are shown in Fig 6.6.

	Equivalence ratio	Inlet condition	Time steps	elapsed time (sec)
Case III	Equivalence ratio - 1	Pressure – 50662.5 pa Temperature – 700 K Mach number – 3.5 Velocity – 2163.944 m/sec	0 to 13000	1.3×10^{-4}
	Equivalence ratio – 0.5	Pressure – 50662.5 pa Temperature – 700 K Mach number – 3.77 Velocity – 2162.29 m/sec	13000 to 18000	5×10^{-4}
	Equivalence ratio – 1	Pressure – 50662.5 pa Temperature – 700 K Mach number – 3.5 Velocity – 2163.944 m/sec	18000 to 24000	6×10^{-4}
	Equivalence ratio – 0.5	Pressure – 50662.5 pa Temperature – 700 K Mach number – 3.77 Velocity – 2162.29 m/sec	24000 to 29000	5×10^{-4}
	Equivalence ratio - 1	Pressure – 50662.5 pa Temperature – 700 K Mach number – 3.5 Velocity – 2163.944 m/sec	29000 to 35200	6.2×10^{-4}

Table 6.3: case III

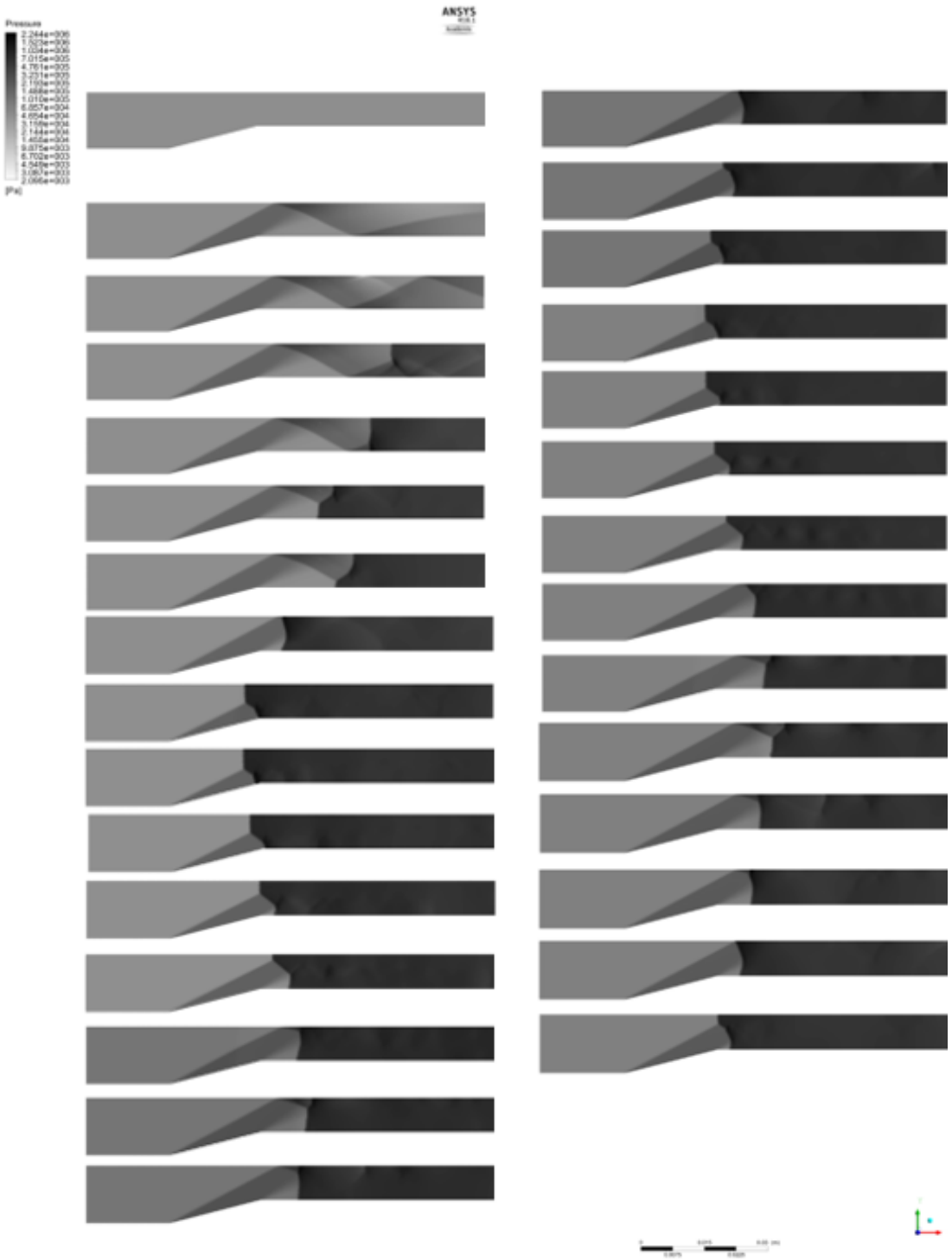

Fig 6.6: Propagation of the flow in case III

Exit condition with respect to time: It is important to check the variation of flow properties at the exit plane with respect to time in the cycle, because the combustion by normal detonation is an unsteady process. By examining the exit conditions of the combustion chamber, with an extended time scale the pressure appears to approach a steady state in case 1. Then by tweaking the inlet condition and equivalence ratio it was made possible to achieve a steady exit plain flow property with an unsteady normal detonation. The Fig 6.7 represents the flow properties at the exit of combustion chamber varying in time for case 1, Fig 6.8 for case 2, and Fig 6.9 for case 3.

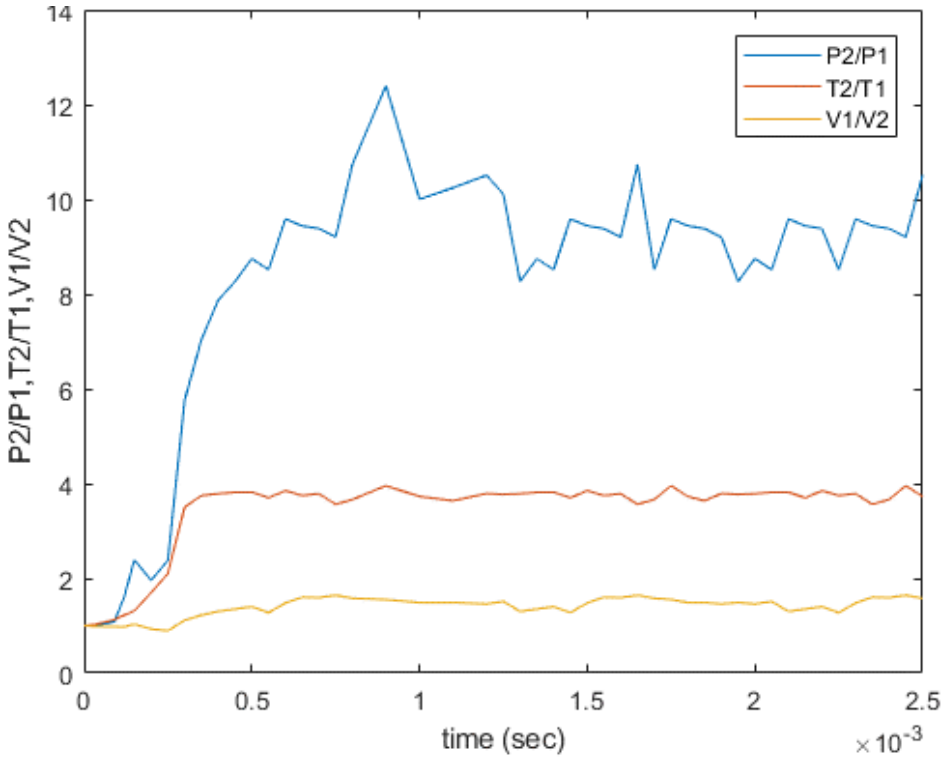

Fig 6.7: Variation of flow properties with respect to time for case I

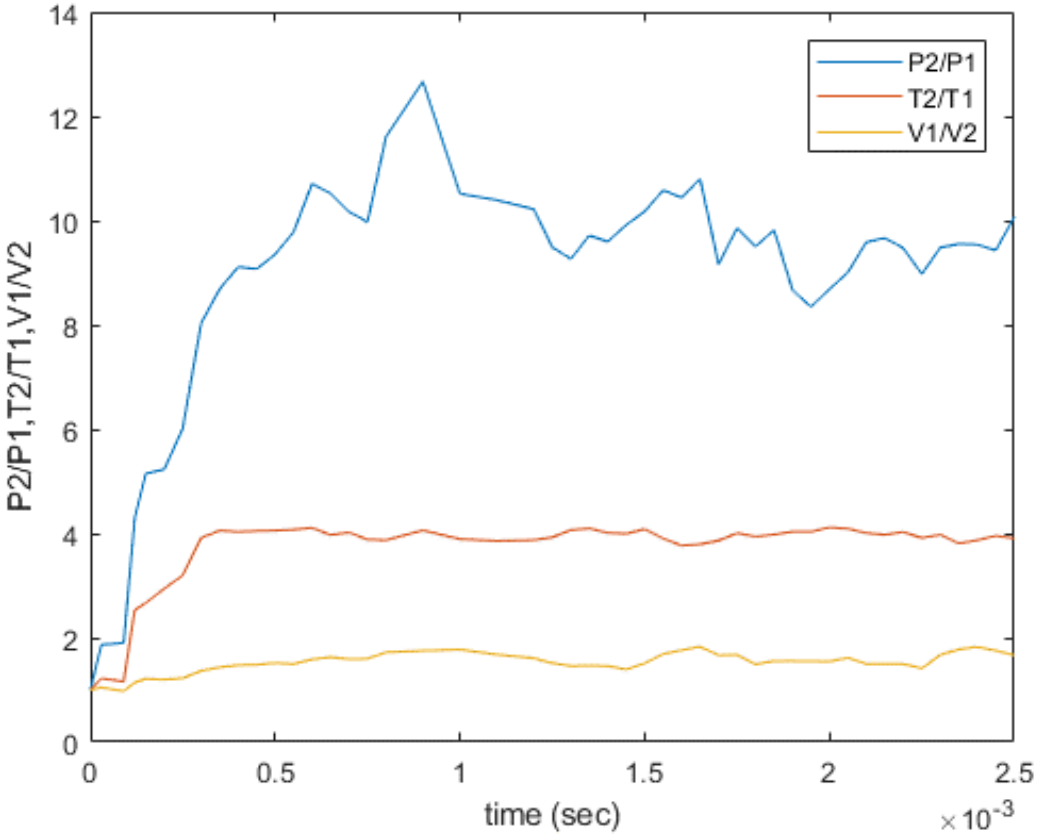

Fig 6.8: Variation of flow properties with respect to time for case II

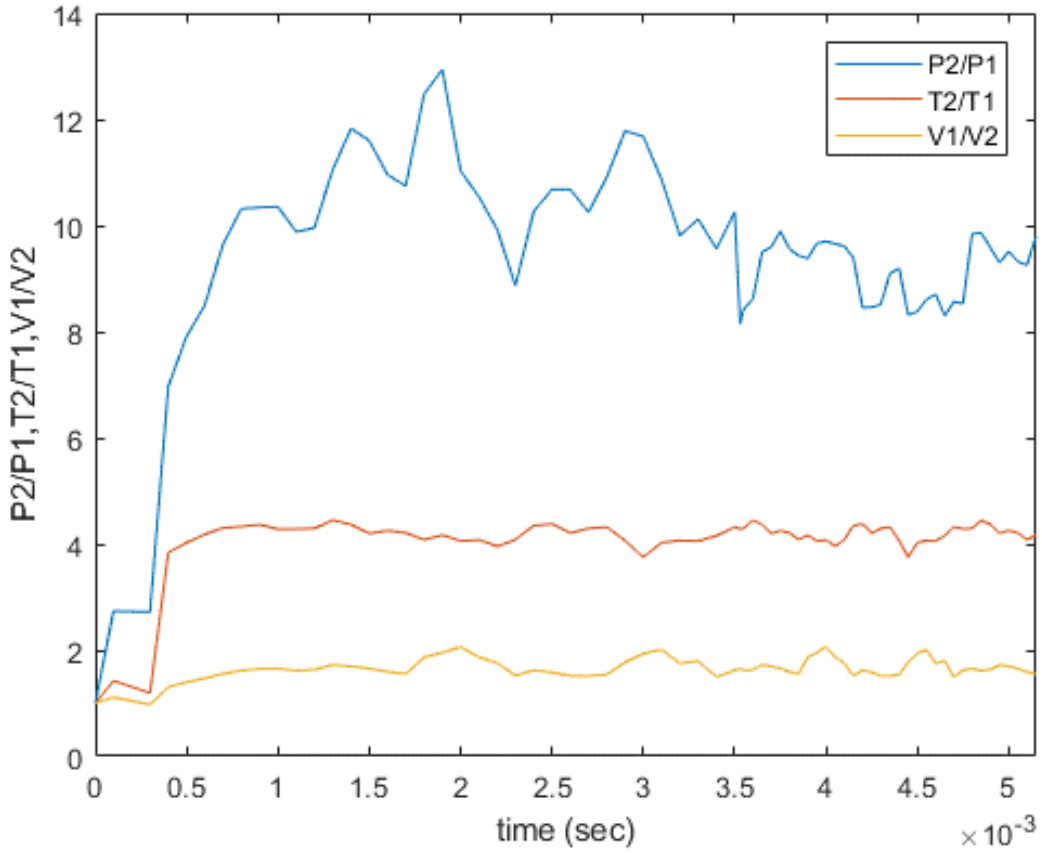

Fig 6.9: Variation of flow properties with respect to time for case III

Chapter 7

CONCLUSION

Simulation of the motion od an unsteady normal detonation combustion wave was evaluated computationally by using Fluent 18.1. The physics of detonation and the chemical reactions were understood and engineered to simulate the cases of unsteady detonation combustion. In the different cases of normal detonation combustion that has been mentioned in chapter 6, the initial flow properties namely the pressure, temperature, and velocity are maintained constant all along the process. The direction of the propagating unsteady detonation wave depends on M_3 as mentioned in chapter 6. The M_3 value is changed by adjusting the mass fraction of the incoming fuel. By controlling the equivalence ratio, the normal detonation wave is made to oscillate inside the combustion chamber. From the elapsed time of each cycle it can be noted that the theoretical frequency that could be achieved by oscillating unsteady detonation wave for combustion is higher than that of the generic Pulsed detonation engine. The theoretical frequency achieved in this detonation combustion is 2200 Hz in Case I, 2170 Hz in Case II and 909 Hz in Case III. This is much higher than the typical 100 Hz frequency that is observed in conventional pulse detonation engine.

From Figs 6.7 – 6.9 it can be inferred that the flow properties at the exit of the combustion chamber are nearly constant even though in the presence of an unsteady normal detonation wave.

As for future work, to find the operating range of the unsteady normal detonation combustion by varying the inlet flow properties namely pressure, temperature and velocity along a typical constant q trajectory. By using different fuels other than hydrogen would provide the ratio of exit to inlet flow properties of the combustion chamber.

APPENDIX A

Fluent Chemkin Input

Reaction Mechanism Input file

```
ELEMENTS
H / 1.00794 /
O / 15.999 /
N / 14.007 /
END
! Species 11
SPECIES
H  H2  H2O  H2O2  HO2  N  N2  NO  O  O2  OH
END

! Reactions 23; A-units (mol-cm-sec)  E-units (cal/mol)
REACTIONS     MOLES         CAL/MOLE
H2 + O2 <=> OH + OH                       1.70E+13        0     47780
OH + H2 <=> H2O + H                       1.17E+09       1.3      3626
O + OH <=> O2 + H                        4.00E+14      -0.5         0
O + H2 <=> OH + H                        5.06E+04      2.67      6290
H + O2 + M <=> HO2 + M                        3.61E+17     -0.72         0
   H2O/18.6/ H2/2.86/ N2/1.26/
OH + HO2 <=> H2O + O2                         7.50E+12         0         0
H + HO2 <=> OH + OH                       1.40E+14        0      1073
O + HO2 <=> O2 + OH                       1.40E+13        0      1073
OH + OH <=> O + H2O                       6.09E+08       1.3         0
H + H + M <=> H2 + M                      1.00E+18        -1         0
   H2O/0./ H2/0./
H + H + H2 <=> H2 + H2                    9.20E+16      -0.6         0
H + H + H2O <=> H2 + H2O                        6.00E+19     -1.25         0
H + OH + M <=> H2O + M                          1.60E+22        -2         0
   H2O/5./
H + O + M <=> OH + M                      6.20E+16      -0.6         0
   H2O/5./
O + O + M <=> O2 + M                      1.89E+13         0     -1788
H + HO2 <=> H2 + O2                       1.25E+13        0         0
HO2 + HO2 <=> H2O2 + O2                         2.00E+12         0         0
H2O2 + M <=> OH + OH + M                        1.30E+17         0     45500
H2O2 + H <=> HO2 + H2                     1.60E+12        0      3800
H2O2 + OH <=> H2O + HO2                         1.00E+13         0      1800
O + N2 <=> NO + N                        1.40E+14         0     75800
N + O2 <=> NO + O                        6.40E+09         1      6280
OH + N <=> NO + H                         4.00E+13         0         0
END
```

Thermodynamics data base

THERMO

300.000 1000.000 5000.000

H 120186H 1 0 0 0G 300.00 5000.00 1000.0 1

2.50000000E+00 0.00000000E+00 0.00000000E+00 0.00000000E+00 0.00000000E+00 2

2.54716300E+04-4.60117600E-01 2.50000000E+00 0.00000000E+00 0.00000000E+00 3

0.00000000E+00 0.00000000E+00 2.54716300E+04-4.60117600E-01 4

H2 121286H 2 0 0 0G 300.00 5000.00 1000.0 1

2.99142300E+00 7.00064400E-04-5.63382900E-08-9.23157800E-12 1.58275200E-15 2

-8.35034000E+02-1.35511000E+00 3.29812400E+00 8.24944200E-04-8.14301500E-07 3

-9.47543400E-11 4.13487200E-13-1.01252100E+03-3.29409400E+00 4

H2O 20387 H 2O 1 0 0G 300.00 5000.00 1000.0 1

2.67214600E+00 3.05629300E-03-8.73026000E-07 1.20099600E-10-6.39161800E-15 2

-2.98992100E+04 6.86281700E+00 3.38684200E+00 3.47498200E-03-6.35469600E-06 3

6.96858100E-09-2.50658800E-12-3.02081100E+04 2.59023300E+00 4

H2O2 120186H 2O 2 0 0G 300.00 5000.00 1000.0 1

4.57316700E+00 4.33613600E-03-1.47468900E-06 2.34890400E-10-1.43165400E-14 2

-1.80069600E+04 5.01137000E-01 3.38875400E+00 6.56922600E-03-1.48501300E-07 3

-4.62580600E-09 2.47151500E-12-1.76631500E+04 6.78536300E+00 4

HO2 L 5/89H 1O 2 0 0G 200.00 3500.00 1000.0 1

4.01721090E+00 2.23982013E-03-6.33658150E-07 1.14246370E-10-1.07908535E-14 2

1.11856713E+02 3.78510215E+00 4.30179801E+00-4.74912051E-03 2.11582891E-05 3

-2.42763894E-08 9.29225124E-12 2.94808040E+02 3.71666245E+00 4

N L 6/88N 1 0 0 0G 200.00 6000.00 1000.0 1

2.41594290E+00 1.74890650E-04-1.19023690E-07 3.02262450E-11-2.03609820E-15 2

5.61337730E+04 4.64960960E+00 2.50000000E+00 0.00000000E+00 0.00000000E+00 3

0.00000000E+00 0.00000000E+00 5.61046370E+04 4.19390870E+00 4

N2 121286N 2 0 0 0G 300.00 5000.00 1000.0 1

2.92664000E+00 1.48797700E-03-5.68476100E-07 1.00970400E-10-6.75335100E-15 2

-9.22797700E+02 5.98052800E+00 3.29867700E+00 1.40824000E-03-3.96322200E-06 3

5.64151500E-09-2.44485500E-12-1.02090000E+03 3.95037200E+00 4

NO RUS 78O 1N 1 0 0G 200.00 6000.00 1000.0 1

3.26060560E+00 1.19110430E-03-4.29170480E-07 6.94576690E-11-4.03360990E-15 2

9.92097460E+03 6.36930270E+00 4.21847630E+00-4.63897600E-03 1.10410220E-05 3

-9.33613540E-09 2.80357700E-12 9.84462300E+03 2.28084640E+00 4

O 120186O 1 0 0 0G 300.00 5000.00 1000.0 1

2.54206000E+00-2.75506200E-05-3.10280300E-09 4.55106700E-12-4.36805200E-16 2

2.92308000E+04 4.92030800E+00 2.94642900E+00-1.63816600E-03 2.42103200E-06 3

-1.60284300E-09 3.89069600E-13 2.91476400E+04 2.96399500E+00 4

O2 121386O 2 0 0 0G 300.00 5000.00 1000.0 1

3.69757800E+00 6.13519700E-04-1.25884200E-07 1.77528100E-11-1.13643500E-15 2

-1.23393000E+03 3.18916600E+00 3.21293600E+00 1.12748600E-03-5.75615000E-07 3

1.31387700E-09-8.76855400E-13-1.00524900E+03 6.03473800E+00 4

OH 0 ruciH 1O 1 0 0G 300.00 5000.00 1710.0 1

2.85376040E+00 1.02994334E-03-2.32666477E-07 1.93750704E-11-3.15759847E-16 2

3.69949720E+03 5.78756825E+00 3.41896226E+00 3.19255801E-04-3.08292717E-07 3

3.64407494E-10-1.00195479E-13 3.45264448E+03 2.54433372E+00 4

END

REFERENCE

[1] Munipalli R., Shankar V, Wilson D.R, Kim H., Lu F.K. and Hagseth P., "A Pulsed Detonation Based Multimode Engine Concept," AIAA Paper 2001-1786, 2001

[2] Lee J. H. S, 2008. The Detonation Phenomenon. Cambridge, New York

[3] Wildon Fickett and William C. Davis, University of California Press, Berkeley - Los Angeles - London, 1979 "Detonation."

[4] Fan H.Y, and Lu F.K, 2008. "Numerical modeling of oblique shock and detonation waves induced in a wedged channel". Journal of Aerospace Engineering, 222(5), pp. 687–703

[5] Jin L, Fan W, Wang K, and Gao Z, "Review on the recent development of multi-mode combined detonation engine," International Journal of Turbo & Jet Engines, vol. 30, no 3 pp. 303–312, 2013.

[6] Heiser W., and Pratt D., "Thermodynamic Cycle Analysis of Pulse Detonation Engines," Journal of Propulsion and Power, vol. 18, no 1, 2002, pp. 68-76.

[7] Bussing T. R. A., and Pappas G., 1996. "Pulse Detonation Engine Theory and Concepts", Vol. 165 of Progress in Aeronautics and Astronautics. AIAA, Reston, Virginia, pp. 421 – 472.

[8] Kim H. W., Lu K.L., Anderson D.A., and Wilson D.R., “Numerical simulation of detonation process in a tube," Computational Fluid Dynamics Journal, vol. 12, no. 2, pp. 227 - 241, 2003.

[9] Rogers R.C. and Chinitz W., “Using a global hydrogen-air combustion model in turbulent reacting flow calculations," AIAA Journal, vol. 21, no. 4, pp. 586 - 592, 1983.

[10] Kee R.J., Rupley F. M., and Ellen Meeks, Thermal and Plasma Processes Department and James A. Miller, Combustion Chemistry Department, “CHEMKIN-III: A FORTRAN chemical kinetics package for the analysis of gas phase chemical and plasma kinetics”, pg. 134

[11] Kee R.J., Miller J.A., and Jereson, \Chemkin: A general purpose problem independent, transportable Fortran chemical kinetics code package," Sandia National Laboratories, Tech. Rep. SAND 80-8003, 1986.

[12] Gordon S. and McBride B.J, “Computer program for calculation of complex chemical equilibrium compositions and application I. Analysis”, Tech. Rep. NASA RP{1311, 1976. [Online]. Available: http://www.lerc.nasa.gov/WWW/CEAWeb

[13] Morley C. GASEQ: A chemical equilibrium program. [Online]. Available: http://www.gaseq.co.uk

[14] Berkenbosch, A. C. (1995). Capturing detonation waves for the reactive Euler equations Eindhoven: Technische Universiteit Eindhoven DOI: 10.6100/IR445469

[15]M. W. Chase, C. A. Davis, J. R. Downey, D. J. Frurip, R. A. McDonald, and A. N. Syverud, “JANAF Thermochemical tables”, Journal of Physical Chemistry, 1985.

[16] J. O. Hirschfelder, C. F. Curtiss, and R. B. Bird, Molecular Theory of Gases and Liquids. New York: John Wiley, 1954.

[17] J. D. Anderson, Hypersonic and High-Temperature Gasdynamics. New York: McGraw-Hill, 1998.

[18] 2013. Ansys fluent text command list. Online, Nov.

[19] Castillo, J. E., 1991. Mathematical aspects of numerical grid generation, Jan

[20] T. H. Yi, D. A. Anderson, D. R. Wilson, and F. K. Lu, 'Numerical study of two - dimensional viscous, chemically reacting flow'," AIAA 2005-4868, 2005.

[21] Anon., 2013. Ansys fluent user’s guide, release 15.0. Tech. rep., ANSYS, Inc.

[22] Texas Advanced Computing Center, The University of Texas at Austin, 2017. Stampede User Guide

[23] Office of Information Technology, The University of Texas at Arlington, 2017. HPC Users Guide

[24] Bussing, T., and Pappas, G., "An Introduction to Pulse Detonation Engines," AIAA Paper 1994-0263, 1994.